Near Infrared Spectroscopy based Brain Computer Interface for Decoding Speech

By

Usman Ayub Sheikh

NUST201362037MSMME62113F

Supervisor

Dr. Syed Omer Gilani

Department of Robotics and Artificial Intelligence

School of Mechanical and Manufacturing Engineering (SMME)

National University of Sciences and Technology (NUST)

Islamabad, Pakistan

February 2016

Near Infrared Spectroscopy based Brain Computer Interface for Decoding Speech

By

Usman Ayub Sheikh

NUST201362037MSMME62113F

Supervisor

Dr. Syed Omer Gilani

Co-supervisor

Dr. Mohsin Jamil

A thesis submitted in conformity with the requirements for the degree of *Master of Science* in Robotics and Intelligent Machines Engineering

Department of Robotics and Artificial Intelligence
School of Mechanical and Manufacturing Engineering (SMME)
National University of Sciences and Technology (NUST)
Islamabad, Pakistan

February 2016

Declaration

I, *Usman Ayub Sheikh* declare that this thesis titled "Near Infrared Spectroscopy based Brain Computer Interface for Speech Decoding" and the work presented in it are my own and has been generated by me as a result of my own original research.

I confirm that:

1. This work was done wholly or mainly while in candidature for a Master of Science degree at NUST
2. Where any part of this thesis has previously been submitted for a degree or any other qualification at NUST or any other institution, this has been clearly stated
3. Where I have consulted the published work of others, this is always clearly attributed
4. Where I have quoted from the work of others, the source is always given. With the exception of such quotations, this thesis is entirely my own work
5. I have acknowledged all main sources of help
6. Where the thesis is based on work done by myself jointly with others, I have made clear exactly what was done by others and what I have contributed myself

---

Usman Ayub Sheikh,
NUST201362037MSMME62113F

Copyright Notice

This thesis is dedicated to *my beloved parents*

Abstract

People suffering from neuromuscular disorders such as tetraplegia are left in a locked-in state with preserved awareness and cognition. Brain-computer interfaces (BCI) can potentially redefine the quality of life of such individuals by allowing them to communicate their intention through modulation of localized brain activity. Near Infrared Spectroscopy (NIRS), a relatively recent BCI modality, can be used to non-invasively monitor such an activity by measuring corresponding changes in cerebral blood oxygenation. In this study, it was hypothesized that the activation of Broca's area due to auditory imagery as conveyed by local hemodynamic activity can be harnessed to create an intuitive BCI based on NIRS. A 12-channel square template was used to cover inferior frontal gyrus and changes in hemoglobin concentration corresponding to six aloud (overtly) and silently (covertly) spoken words were collected from 8 healthy subjects. The features extracted from each of the trials using unsupervised feature learning were classified with an optimized support vector machine. The results showed large intra- and inter- subject variability. For all subjects, when considering overt and covert classes regardless of words, classification accuracy of 95.83% (±5.87%) was achieved with deoxy-hemoglobin (HHb) and 94.22% (±6.87%) with oxy-hemoglobin (O2Hb) as a chromophore. For a six-class classification problem of overtly spoken words, 66.48% (±17.07%) accuracy was achieved for HHb and 58.90% (±27.68%) for O2Hb. Similarly, for a six-class classification problem of covertly spoken words, 70.07% (±12.11%) accuracy was achieved with HHb and 65.91% (±16.89%) with O2Hb as an absorber. These results indicate that a control paradigm based on covert speech can be reliably implemented into future BCIs based on NIRS.

Keywords: *Brain computer interface, near infrared spectroscopy, covert speech, unsupervised feature extraction, Broca's area*

Acknowledgments

Endless gratitude and thanks to Allah Almighty who bestowed mankind with the light of knowledge through laurels of perception, learning and reasoning.

A number of people have directly or indirectly contributed to the realization of this thesis, I would like to take this opportunity to express my sincere thanks to every one of them.

First and foremost, I would like to extend my deepest gratitude to my advisor, *Dr. Syed Omer Gilani*, for his professional guidance, insightful commentary and thorough support throughout the course of this work. I am very thankful to him for the long discussions that helped me sort out the technical details of this project. I am also thankful to him for encouraging the use of correct terminology and consistent notation in my writings and presentations.

I am extremely indebted to *Dr. Ernest Nlandu Kamavuako* and his team at Center for Sensory-Motor Interaction, Aalborg Universitet, Denmark for their generous sharing of data, time and valuable feedback at every turn. I would also like to extend my appreciation to *Jakob Celander Rosenvang* – one of Dr. Ernest's graduate students – for a comprehensive report documenting every relevant detail about the dataset and the experimental design.

Acknowledgment is also due to *Dr. Imran Khan Niazi*, Center for Chiropractic Research, New Zealand College of Chiropractic, his clinical insight and practical advice turned out to be extremely useful and invaluable for this thesis.

Last but not the least, I would like to express my heart-felt gratitude to my family and friends. They have been a constant source of love, concern, support and strength throughout my graduate studies.

Contents

List of Figures

List of Tables

List of Abbreviations and Symbols

Abbreviations

LIS	Locked-in Syndrome
QoL	Quality of Life
BCI	Brain-computer Interface
EEG	Electroencephalography, Electroencephalographic
NIRS	Near Infrared Spectroscopy
MRI	Magnetic Resonance Imaging
fMRI	Functional Magnetic Resonance Imaging
BOLD	Blood-oxygenation Level Dependent
O2Hb	Oxygenated Hemoglobin
HHb	Deoxygenated Hemoglobin
ALS	Amyotrophic Lateral Sclerosis
LQ	Laterality Quotient
IFG	Inferior Frontal Gyrus
PCA	Principal Component Analysis
FLDA	Fisher's Linear Discriminant Analysis

SVM	Support Vector Machine
MI	Motor Imagery
DPF	Differential Path Length Factor

Chapter 1

Introduction

Locked-in syndrome (LIS) is a neuromuscular disorder described as near-complete paralysis with preserved awareness and cognition [5]. Its patients are left with very few degrees of freedom ranging from restricted eye movement (classic LIS) to complete immobility (total LIS) [6]. The most common cause of LIS is a stroke or a traumatic brain injury (31%) or a cerebrovascular disease (52%) [7]. According to [8], more than half a million people worldwide are affected by LIS. Once an LIS patient has become medically stable, his/her life span can be significantly prolonged. With very minor chances of motor recovery and so poor quality of life, healthy individuals and medical experts often find themselves wondering if such a life is worth fighting for [9]. Recent advances in brain-computer interfaces (BCI) can potentially redefine the quality of life (QoL) for such patients by providing them with muscle independent communication channel to communicate and interact with their environment.

When considering a BCI for a speech-deprived patient, one must also take into account the nature of the patient's impairment. Interfaces that rely on movement of non-vocalized articulators or reliable control of muscles for restoration of speech are not feasible for those suffering from LIS. Non-invasive BCIs currently available for such patients are mostly limited to those based on Electroencephalographic (EEG) signals [10]. While EEG based BCIs have been in use for a long time now, their clinical efficacy has clearly been limited by their technological limitations [11]. For one, such interfaces require the patients to spend months to train themselves how to consciously modulate their EEG activity and even then high error rates are not avoidable [12]. An alternative technique based on *Near Infrared Spectroscopy (NIRS)* that involves monitoring neu-

ronal activity based on changes in hemodynamic response can be used to create BCIs that require very little user training and thus prevent the drawbacks associated with EEG based BCIs. In this study, it has been investigated if an intuitive BCI based on NIRS can be created for those suffering from neuromuscular disorders such as LIS to improve their QoL.

The primary objective of this thesis is to work out the feasibility of detecting user's intention by decoding his/her speech. If a small set of overtly/covertly said words can reliably generate hemodynamic activity discernible with NIRS, then a control paradigm based on speech may be implemented into future NIRS-BCIs. In order to achieve this objective, several choices related to signal acquisition and speech classification were made, among them are

1. As *Broca's* area (speech center) plays an important role in speech processing [13] and as activation within this area is unavoidable during speech [14], it was chosen to focus on just this area.

2. Since a navigational approach allows an intuitive control for most BCI applications – selection of letters on a virtual keyboard [15] or navigation of a mouse [16] or a wheelchair [17] – it was chosen to use six directional words i.e. 'up', 'down', 'right', 'left', 'forward' and 'backward' to make the control as intuitive as possible.

To our best knowledge, exploiting the advantages of NIRS for identification of multiple distinct outcomes from speech on a relatively localized area – Broca's area – as a control scheme for a BCI forms a novel approach.

The following chapter i.e. Chapter 2 presents a brief overview of brain anatomy and physiology and covers functional areas whose appreciation is fundamental to the understanding of this study. A concise review of functional neuroimaging techniques with a focus on non-invasive BCIs has been given in Chapter 3. Chapter 4 describes the experimental design including details related to subjects, tasks and protocol for the study. This brings us to Chapter 5 which presents background material related to artifact removal and feature extraction of NIRS signals. Chapter 6 details the signal processing and speech classification pipeline that has been followed in order to achieve the best possible classification performance and finally, Chapter 7 concludes the thesis with a discussion of results and future prospects.

Chapter 2

Brain Anatomy and Physiology

2.1 Organization of the Brain

The center of our nervous system – the most sophisticated neural network – the human brain accounts for about 98% of the body's neural tissue and weighs about 1.4 kg with large individual variance [18]. It is an upper, enlarged end of the spinal cord and can gross anatomically be subdivided into four parts; namely, the brainstem, the diencephalon, the cerebellum and the cerebrum [19] (Figure 2.1, Figure 2.2a).

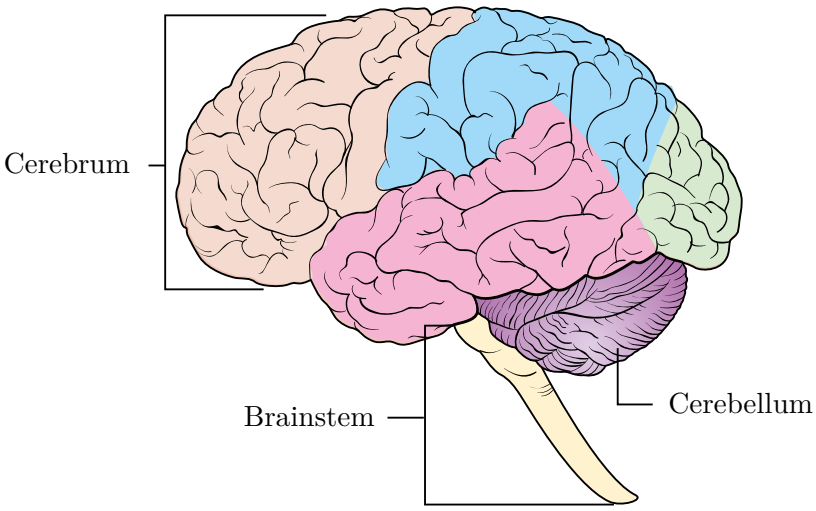

Figure 2.1: The principle parts of the brain. Retrieved from [1]

2.1.1 The Brainstem

Connected to the spinal cord, the brainstem is located in the most inferior part of the brain and consists of medulla oblongata, pons and mesencephalon (Figure 2.2a). The medulla is considered as the most important part of the brain because of the myriad of crucial involuntary tasks it performs ranging from regulating blood pressure and breathing to transfer of neural messages from brain to the spinal cord. Pons refers to the area that sits directly above the medulla and plays a role of a message center between several areas of the brain including superior parts of the brainstem and the cerebellum. The third part of the brainstem, the mesencephalon – also known as mid-brain – connects pons and cerebellum with cerebral hemispheres, controls auditorily and visually provoked reflexes and helps maintain consciousness. [20, 21]

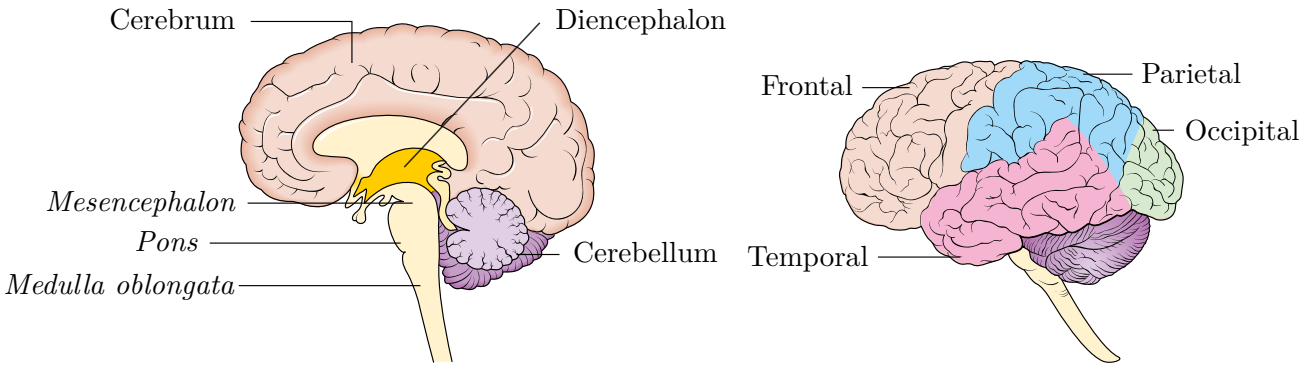

Figure 2.2: (a) The gross anatomy of the brain with a closer look at the brain stem. (b) The four lobes of the cerebral cortex. Both figures are retrieved from [1]

2.1.2 The Diencephalon

Next higher region of the brain, the diencephalon (Figure 2.2a) is made up of three parts including thalamus and hypothalamus. While right and left thalamus are responsible for relaying and processing sensory information, hypothalamus is involved with hormone production, emotions and autonomic function. [20, 22]

2.1.3 The Cerebellum

The cerebellum (Figure 2.2a), also known as hind-brain, is located at the level of the mesencephalon and is covered by the cerebellar cortex. It plays an important role in motor control by subconsciously coordinating repeated advanced somatic motor pat-

terns in response to the sensory feedback it receives from ligaments, joints, muscles, the vestibular system of the ears etc. Tumors in this part of the brain can cause loss of balance, precision and difficulty in coordinating movements. [23, 24]

2.1.4 The Cerebrum

The cerebrum (Figure 2.2a), also known as the fore-brain, is the superior-most region of the brain and is made up of two highly folded cerebral hemispheres – right and left – separated by a longitudinal fissure. It controls higher mental functions such as thinking, memory, emotions, highly complex movements, senses and *speech*. The superficial layer of the cerebrum – known as cerebral cortex – may be classified on the basis of gross topography into four lobes i.e. frontal lobe, parietal lobe, occipital lobe and temporal lobe (Figure 2.2b). Each of these lobes can be considered to have specific function though the brain is too complicated and interlinked for such functional lines to be drawn. The cerebral cortex – also referred to as 'gray matter' – consists of several areas including motor/sensory cortices, association centers and integrative centers. [23, 24]

Cortices

The primary motor cortex – located in the posterior region of the frontal lobe – works in cooperation with other motor areas such as premotor cortex to plan and direct voluntary movements. Posterior to this cortex is the primary somatosensory cortex which is located in the parietal lobe. This cortex allows a conscious perception of touch, pain and pressure etc. The two cortices are referred to as primary because they have a well-defined topographic mapping of the body e.g. a specific area of the primary motor cortex is related to motion of the arm, similarly, the superior end of the two cortices corresponds to the feet and the inferior accounts for the head. The gustatory cortex, located in the frontal lobe, is responsible for the sensation of taste. Visual cortex, as its name would suggest, is responsible for processing of visual information it receives from eyes. The auditory and olfactory cortices, both located in the temporal lobe, are related to sound and smell respectively. [19, 23]

Association Centers

In addition to these cortices, there are association centers that help in interpretation of sensations and coordination of motor responses. So, if the visual association center is damaged, the person may be able to look at a cat but not identify/recognize it as one. In a similar way, while primary motor cortex's job is to initiate the actual movement, it is the responsibility of motor association center to relay proper instructions to it in order to bring about smooth and skilled movement. The somatic sensory association center is linked to the primary somatosensory cortex and allows recognition of touch. The same is true for each of the remaining cortices. [19, 22, 23]

Integrative Centers

The cerebral cortex also contains areas that retrieve information from several association centers in order to perform highly complex motor or analytical activities. One such center is the prefrontal cortex located in the frontal lobe, which integrates information from sensory association centers and achieves various intellectual functions. Another integrative center, Wernicke's area (Figure 2.3) is located in one of the two hemispheres and is responsible for integrating sensory information while allowing coordinated access to visual and auditory memory. So, while words of a sentence might separately be understood by an association center, it is Wernicke's area that interconnects them into a whole meaningful sentence. [19, 23]

2.2 The Speaking Brain

2.2.1 Hemisphere Lateralization

Even though the two hemispheres look identical in terms of structure, each of them operates in an entirely different way and is responsible for very different activities. This is known as hemisphere lateralization [19, 22]. In most people, the general interpretive areas and specialized language areas exist in the left hemisphere. While this holds true for 97% of right-handed people, 19% of left-handed people have their language centers in the right hemisphere and nearly 12% of them have bilateral lateralization [25].

2.2.2 Broca's Area

Broca's area (Figure 2.3) or the speech center, an integrative center located near Wernicke's area, integrates all the processes needed to vocalize words such as breathing and muscle control. This region also receives auditory feedback from the auditory association center allowing quick adjustments to further vocalization [23].

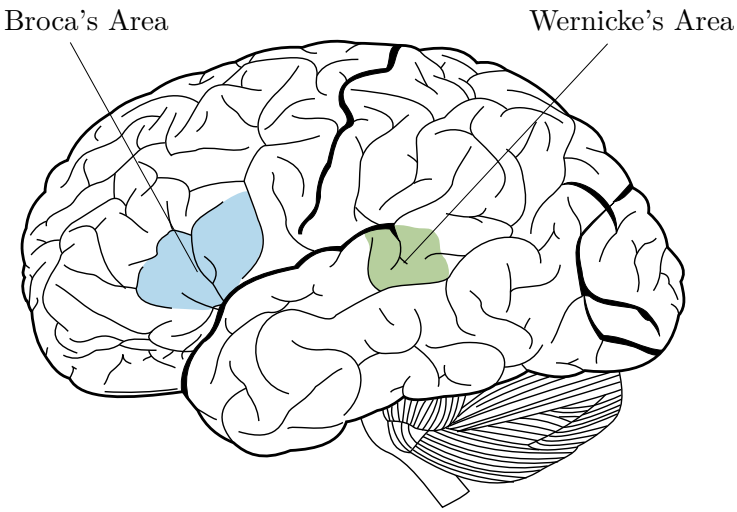

Figure 2.3: The speech areas of the brain. Retrieved from [2]

Damage to this area often results in Broca's aphasia – a speech disorder described by non-fluent and slurry vocal communication with relatively preserved language comprehension [26]. In spite of that, the research evidence regarding the relationship between Broca's area and speech-related functions is quite controversial. While a significant number of studies suggest that lesions in Broca's area do not always lead to Broca's aphasia [27, 28], equally strong research evidence shows that patients with Broca's aphasia do not always have a lesion in their Broca's area [29]. Similarly, whereas numerous functional neuroimaging studies have reported activation of Broca's area due to language-related tasks [30, 31], number of research outcomes supporting activation of Broca's area by non-language-related tasks is not insufficient either [32, 33].

In this study, it has been investigated if the activation of Broca's area due to a set of overtly/covertly spoken words as conveyed by hemodynamic activity can be harnessed to create an intuitive BCI based on NIRS.

Chapter 3

A Review of Functional Neuroimaging Techniques

Functional neuroimaging refers to the use of neuroimaging technique such as Magnetic Resonance Imaging (MRI) to measure a facet of brain function in order to understand the relationship between measurable activity in specific brain areas and corresponding functions. Among well-known and commonly used functional neuroimaging technologies are: Functional Magnetic Resonance Imaging (fMRI), Electroencephalography (EEG) and Near Infrared Spectroscopy (NIRS).

3.1 Functional Magnetic Resonance Imaging (fMRI)

Functional Magnetic Resonance Imaging (fMRI) makes use of the relationship between neural activity and local hemodynamics – cerebral blood flow – to non-invasively capture brain activity [34, 35]. The primary form of fMRI uses Blood-oxygenation Level Dependent (BOLD) [36] response as a measure of neuronal activity. Physiological phenomena that contribute to BOLD response include:

1. Activation of an area within the brain triggers an increase in local blood flow in order to compensate for the enhanced metabolic activity,
2. Magnetic properties of oxygenated hemoglobin are such that it gives rise to a slightly higher MR response than deoxygenated hemoglobin.

By combining these two effects, it can be assured that the MR response corresponding to an activated area is relatively higher than that related to an inactive area. [37]

In spite of the fact that BOLD is an indirect measure, the strong correlation between local neural activity and the corresponding BOLD response as reported in [34, 38] provides a sufficient basis for its use in BCI studies. Studies that have been reported so far include those related to: the effect of deliberate control of anterior cingulate cortex[1] (ACC) on emotional processing [39], the ability of a person to self-regulate his/her BOLD response during language processing [40], the binocular rivalry – a phenomenon of visual perception – in which a face and a house stimulus were presented to different eyes [41] and many others [42, 43].

Although fMRI-BCI allows non-invasive imaging of brain activity in very specific areas of cortical and subcortical regions and is harmless, its clinical utility has largely been limited due to prohibitive costs and complexity of use and development [44].

3.2 Electroencephalography (EEG)

Electroencephalography (EEG), mostly a non-invasive technique, relies on ionic currents – caused by information exchange of neurons – in order to capture the electrical activity of the brain [45]. The activation of a single neuron produces too small a current to be measurable; thus, EEG data always reflects a synchronized electrical activity of multiple active neurons with similar spatial orientation [46]. The main advantage of electro-physiological techniques like EEG is that they can detect brain activity with a very high temporal resolution – an order of magnitude better than fMRI [47]. Spatial resolution is lower than that of fMRI but source analysis can be used to help localize various mental activities [48].

Excellent temporal resolution makes EEG an ideal choice for detection of spatio-temporal distribution of various higher-order cognitive processes such as language functions [49]. Results from BCI studies have shown that people suffering from LIS can learn to modulate their EEG waves – μ and β – in the absence of any perception and movement and can exploit this control as far as to move a cursor on a screen [50] or control an

[1] Located in the medium wall of each hemisphere, this region is connected to the prefrontal cortex, the parietal cortex as well as the motor and visual systems.

electro-stimulation device to grasp a glass of water [51]. Though a number of attempts have been made toward silent speech communication too [52–57], but most of them rely on the user's ability to choose letters on a virtual keyboard through electro-physiological feedback corresponding to 'yes'/'no'. That is to say, these techniques expect accurate visual perception which is an impractical assumption for those with unreliable visual perceptual abilities.

Since EEG only measures the electrical activity of the brain, no health risk is associated with it [58]. A set of small metal electrodes with processing hardware including amplifiers and anti-aliasing filters embedded into an EEG cap make the whole system relatively portable and cheaper as compared to e.g. fMRI [59]. While such advantages make EEG very popular in BCI research, its limited bandwidth [60], steep learning curve [61], susceptibility to electrical interference [62] and performance deterioration over the course of a session [63] make its clinical utilization quite infeasible.

3.3 Near Infrared Spectroscopy (NIRS)

Near Infrared Spectroscopy (NIRS), a relatively recent non-invasive technique [64, 65], makes use of electromagnetic radiation in near-infrared region – 650–900 nm [66] – in order to measure functional activation in cortical areas 1–3 cm beneath the scalp [67]. Among dominant chromophores that also happen to be biologically relevant markers for brain function are: oxygenated (O2Hb) and deoxygenated hemoglobin (HHb) [68]. A typical NIRS instrument is made up of NIR sources by which a biological tissue of interest is irradiated and detectors that receive the light after its interaction with the tissue. Such an interaction between photons and tissue results in three different effects; namely, reflection, scattering and absorption [69]. While reflectance is highly dependent on the angle of the beam of photons and the regularity of the tissue surface and scattering is a function of tissue composition, the amount of absorption is influenced by molecular properties of tissue within the light path [70]. It is through analysis of the influence of these interactions on the properties of received light that physiological changes can be quantified/measured [71].

Currently, there are two distinct classes of methods/data for studying the activity of the brain i.e. 1) a fast optical response directly arising from a neuronal activity and 2) a slow

hemodynamic/metabolic response arising from changes in oxygen consumption caused by a mental activity [72]. Research over the past few years has proven repeatedly that the fast optical response is not a reliable measure of a neuronal activity owing to the fact that it is prone to contamination from other physiological artifacts [73, 74]. As for the slow hemodynamic oscillations, it has been observed that changes in concentration levels of O2Hb/HHb are strongly related to changes in light absorption associated with a localized activation of a cortical region and can be calculated from the attenuation of received light using Modified Beer-Lambert Law [10, 66, 75].

NIRS has emerged during the last decade as a promising non-invasive neuroimaging technique and has been used to map different areas of the brain including primary motor cortex [76], visual stimulation [77] as well as cognitive and language functional areas [65, 78–85]. [86] presents a study conducted on 40 Amyotrophic Lateral Sclerosis (ALS) patients including 17 in locked-in state in order to investigate the use of high-level cognitive tasks as a control signal for a BCI. Single-channel measurements were recorded over the prefrontal cortex while participants performed mental tasks corresponding to 'yes'/'no' in response to a series of questions. Instantaneous amplitude and phase of the NIRS signal were selected as features and a non-linear discriminant classifier was used to achieve an average classification accuracy of 80% (for 23 out of 40 subjects). While EEG-BCIs haven't succeeded in breaking the silence of Completely Locked-in[2] (CLIS) patients [87], a recent clinical study [88] presents a Class IV case evidence proving that NIRS-BCIs could significantly improve the QoL of such people by allowing them to regain basic communication.

Unlike fMRI, NIRS does not constrain users to a restricted range of motion [89] and as opposed to EEG, it is neither susceptible to electrical interference from surroundings nor prone to contamination due to muscle artifacts [90]. The ability to measure functional activation from a series of cognitive tasks opens the door to a range of alternative control schemes involving less user training and thus avoiding the exhausting learning process commonly associated with EEG-BCIs [91]. Keeping in view these advantages of NIRS and the recent success that has accompanied its use in numerous BCI studies involving LIS patients, this study proposes a BCI control paradigm based on overt/covert speech for a non-invasive measurement of metabolic signals using NIRS; moreover, it also investigates if Broca's area is an optimal recording site for such a BCI.

[2] Also referred to as 'total LIS'.

Chapter 4

Experimental Design

In this study, it has been hypothesized that the *hemodynamic activity* generated in *Broca's area* in response to a small subset of *overt/covert speech* is discernible with *NIRS* and can be harnessed to create a *BCI* for those suffering from *neuromuscular disorders* such as LIS. The details related to the participants and the protocol of an experiment that has been devised in order to test this hypothesis have been presented in the following sections.

4.1 Participants

Since the issue of language representation in bilinguals is still a topic of debate [92], it was chosen to include only those subjects that are *monolingual speakers*. A total of 8 *healthy* subjects were selected for the study. These include 6 men and 2 women of mean age 25 (range: 23–29) with *Danish* as their native as well as primary language.

As hemispheric language lateralization varies significantly among left-handed people (refer to § 2.2.1), a quantitative measure known as *Edinburgh Inventory Test* [93] was used to assess the handedness of the participants. The analysis indicated 5 of the subjects to be right-handed with Laterality Quotient (LQ) > 70, 2 to be both-handed (LQ = 10 and 30) and 1 to be left-handed (LQ = -58).

4.2 Protocol

Since no NIRS study to date has compared the effects of both overt and covert speech on Broca's area, it was chosen to use both of these methods. Whereas the use of fMRI for tasks requiring overt speech [94, 95] has largely been limited due to motion and magnetic susceptibility artifacts, similar studies based on NIRS [96] have reported favorable outcomes. Moreover, studies such as [85] have shown NIRS to be useful for covert speech tasks too.

4.2.1 Instrumentation

The experiment was conducted in a dimly lit room. In order to minimize interference due to low-frequent Mayer wave ($\sim$ 0.1 Hz) [97], participants were comfortably seated in a tilted position (40° from upright) with their eyes closed. When prompted to open their eyes, they were able to see the screen. Participants were instructed not to move throughout the experiment as this might produce motion artifacts and thus undesirably disturb the blood flow.

A 12-channel square template (6×6 cm^2) with an interoptode distance of 3 cm was used to cover left inferior frontal gyrus (IFG). To locate in a specific Broca's area, the international 10-20 standard for EEG (Figure 4.1) was used and the template was placed with T3 on one end and F7 on the other (Figure 4.2). This is done in accordance with [98] which has shown F7 to cover anterior portion of pars triangularis[1] and T3 to be posterior to IFG. The area of the template was inspired by [99] which has shown the size of Broca's area to be below 6 cm.

4.2.2 Task

The experiment (Figure 4.3) was composed of two blocks with a 5 min break between them so as to collect as many trials as possible while allowing some time for relaxation too. Each block was composed of a selected set of directional words – 'up', 'down', 'right', 'left', 'forward' and 'backward' in Danish (Table 4.1) – overtly and covertly said for 30 s, at a frequency of 1 Hz.

Within a block, the order of the sessions as well as words (or events) were randomized.

[1] It occupies the triangle-shaped part of the IFG and is one of the subregions of Broca's area.

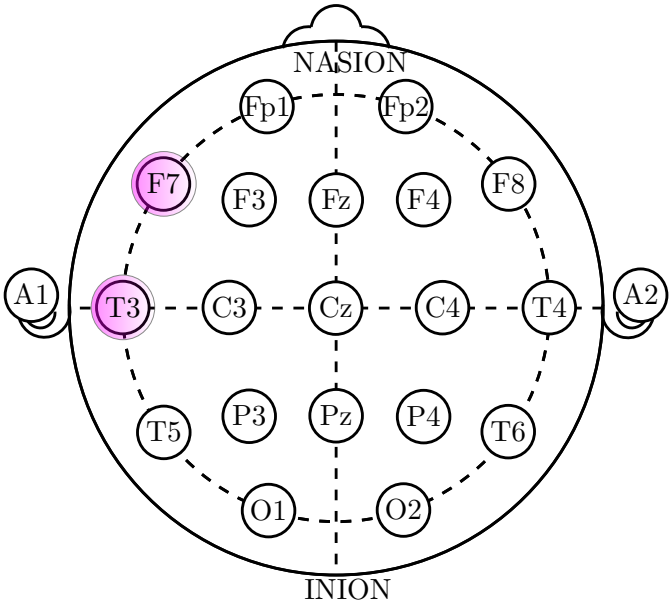

Figure 4.1: The international 10-20 standard for EEG electrode placement as seen from above, where A stands for auricle, C for central, F for frontal, Fp for frontal-pole, O for occipital, T for temporal and z – in Fz, Cz and Pz – for mid-line electrodes. Retrieved from [3].

Danish	English
OP	UP
NED	DOWN
HØJRE	RIGHT
VENSTRE	LEFT
FREM	FORWARD
TILBAGE	BACKWARD

Table 4.1: A list of Danish words that were overtly/covertly spoken during each of the sessions and their English translation

A 1 min break was allowed between words to avoid any carry-over effect; similarly, an additional pause of 1 min was also added before each overt/covert session. Each block thus lasted for about 22 min and a complete experiment had a duration of about 49 min excluding mounting time.

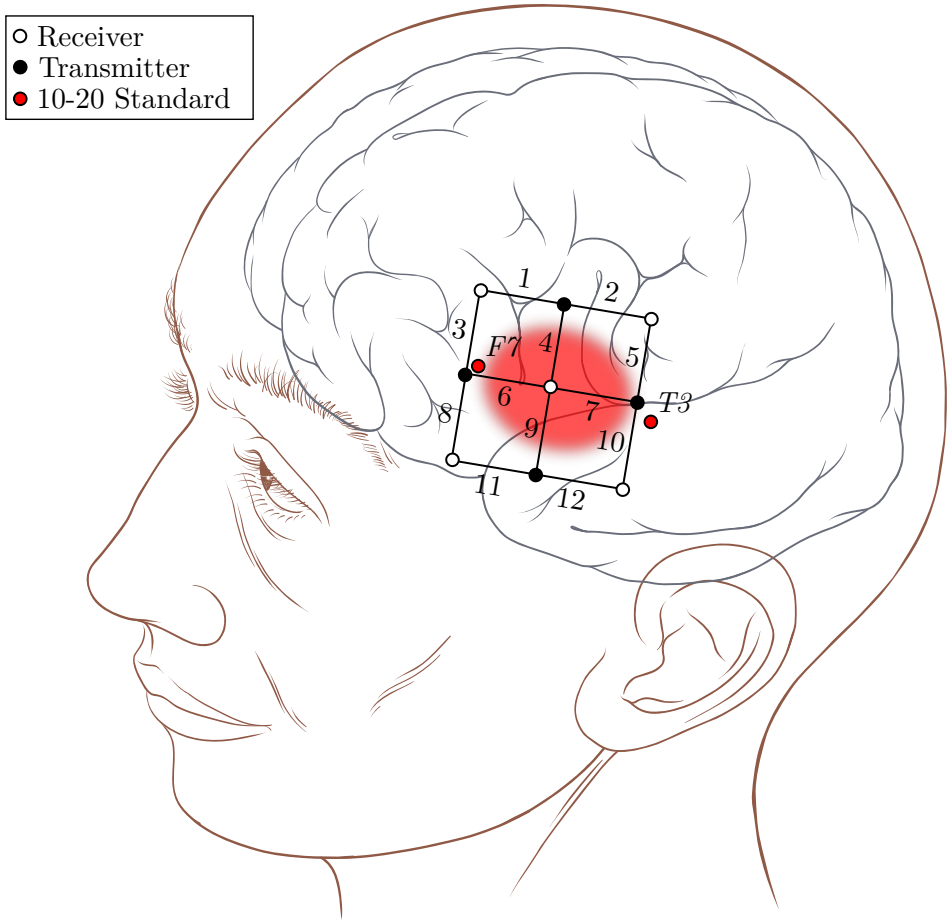

Figure 4.2: A 12-channel square patch with an interoptode distance of 3 cm was placed with T3 on one end and F7 on the other. An estimation of the underlying anatomical structures is also shown with Broca's area highlighted. Retrieved from [4].

4.2.3 Stimulus

The subjects were guided through the experiment by a low-frequent sound (300 Hz, 0.5 s duration) that instructed them to open their eyes, read the word and either overtly or covertly say the word. The sound was played at a low volume to avoid shocking the subjects. The screen also had a 1 Hz counter/indicator to guide the subjects to maintain a constant pace of one word per second. After each event (30 s interval), the screen would go black to signal a break and subjects were instructed to close their eyes and rest. The overt/covert switch and the termination of the block were indicated on the screen by stating 'overt'/'covert' and 'block' respectively after 1 min of black screen.

The procedure based on such an audio-visual instruction was chosen so as to minimize the activity in the IFG and its surroundings by maximizing the use of the visual cor-

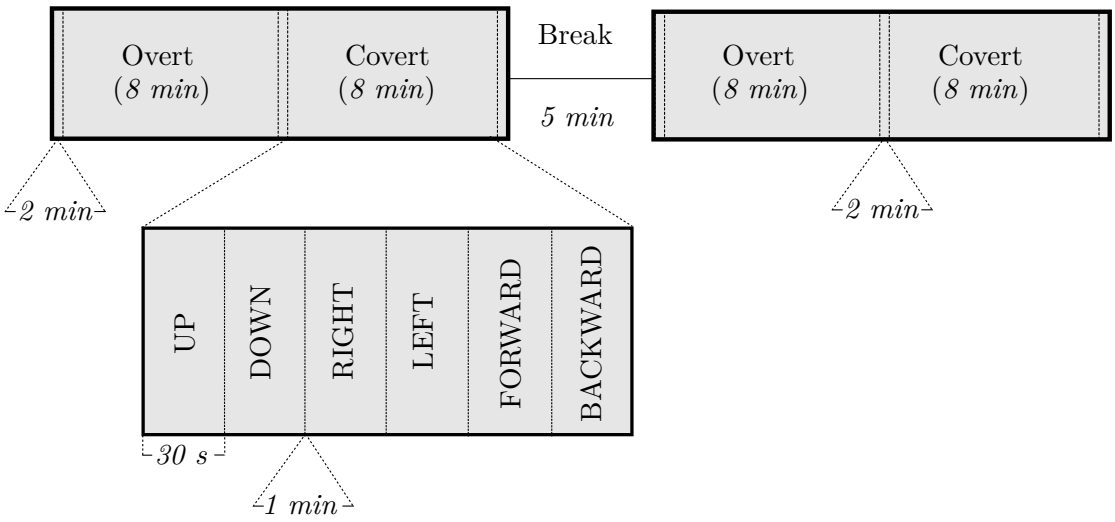

Figure 4.3: An example of the experiment layout showing the overt/covert sessions (8 min) alternating with the relaxation periods (2 min) and a zoomed-in view of the speech events within one session. Note: The figure is not drawn to scale.

tex – in the occipital lobe – and minimizing the use of the auditory cortex – in the temporal lobe, close to T3. Similarly, during covert speech trials, it was ensured that the subject does not make mouth movement as this might induce additional changes in cerebral hemodynamics [100] and thus disturb the response associated with a particular activation trial. Prior to the experiment, it was also confirmed that the subject could easily hear the sound and is familiar with the task and the stimulus of the experiment but is unaware of the true purpose of the study as knowing this much might disturb the validity of the results.

Chapter 5

Classification of NIRS Signals

The core of a BCI is a classification algorithm that maps brain signals into a space of signal descriptors, also known as feature vectors and assigns each of them to a class/label. Given a set of feature vectors and corresponding labels, a supervised classification algorithm splits it into two folds i.e. training and testing. Whereas the training set – labeled feature vectors – is used to learn decision boundaries that separate one class from the other, the testing set – unseen/unlabeled feature vectors – is used to evaluate the performance of the learned model.

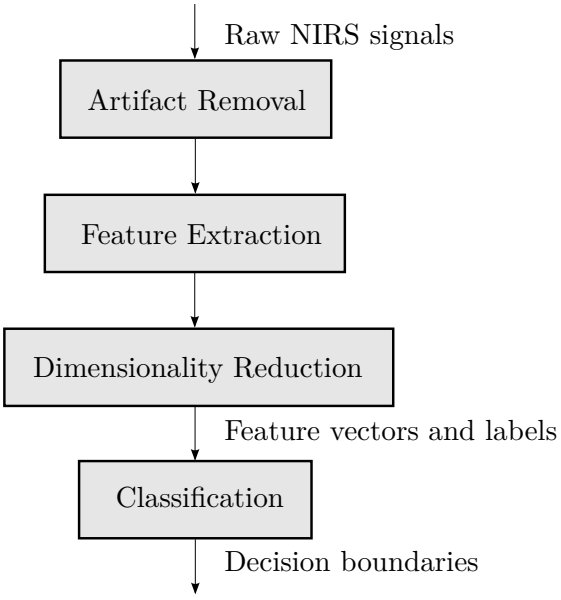

Figure 5.1: Steps involved in preprocessing and classification of NIRS signals

Algorithms proposed for classification of NIRS signals vary in complexity ranging from simple thresholding [101] to statistical model-based approaches [67] and are not quanti-

tatively comparable across studies as every research is based on different control scheme and experimental design. This chapter presents a brief overview of different processes that are generally involved in the preprocessing and classification of NIRS signals, these include artifact removal, feature extraction, feature selection or dimensionality reduction and classification (Figure 5.1).

5.1 Artifact Removal

Among a number of physiological phenomena that contribute to noise in cerebral hemodynamic response are respiration, cardiac activity and motion artifacts [102, 103]. While removal of these effects is necessary in order to ensure that the data is well prepared for further processing, it is impossible to guarantee that it would not cause a loss of valuable information. Moreover, since the amount of physiological noise has been found to vary across subjects as well as experimental setups [104], a preprocessing scheme that works for one study might not be feasible for another one. Nevertheless, over the passage of time, a number of signal enhancement methods have been proposed for NIRS, these include spectral filtering, adaptive filtering, linear detrending, wavelet minimum description length detrending and singular spectrum analysis [105–107].

5.2 Feature Extraction

Feature extraction involves transformation of a signal into such numerical attributes that are not only non-redundant but also sufficiently informative. Among several features that can be used to represent changes in hemoglobin concentration within a trial[1] are mean, variance, skewness and kurtosis of a NIRS signal. [108] used a best combination of these on a specific channel to differentiate between simple and complex imaginary finger tapping and achieved an average accuracy of 81% across 12 subjects. Similarly, [83] used a folding average – an average response of four blocks of data constituting repetitions of language translation tasks – to compare tasks such as translation from foreign to native language, vice versa and a simple read-aloud across 8 Dutch students. The between-person variability in timing and amplitude of the hemodynamic response leaves such time-window based approaches at a disadvantage and calls for an in-depth

[1] An analysis interval or a time window.

investigation of other time-domain features. It has also been shown in [109, 110] that time-frequency domain features can easily be used to separate task-related components of the signal and thus achieve high classification accuracy.

5.3 Dimensionality Reduction

Even if a combination of 3 features e.g. mean, variance and skewness is used to represent a single channel, one time-window comprising of 12 channels can yield up to 36 values (refer to § 4.2.2 and § 4.2.3). Such a high-dimensional feature-space can create a number of problems related to analysis and organization of data mostly due to sparsity and redundancy of variables. These nonintuitive issues are often referred to as the curse of dimensionality and can be prevented by reducing the feature-space to include only the most relevant and discriminant dimensions without a loss of valuable information.

Among well known dimensionality reduction methods are Principal Component Analysis (PCA) and Linear Discriminant Analysis (LDA). While both of these statistical procedures can transform a set of possibly correlated features to a lower dimensional space of uncorrelated variables, they are linear approaches and thus assume the feature-space to be representable as a linear combination of subspaces [111]. In real-world problems, one rarely has the luxury of knowing so much about the relationships in data which necessitates the use of methods that are independent of the structure of the feature-space and are sufficiently reliable at the same time. [112, 113] and [114] propose a number of such randomized algorithms and also present a few numerical examples so as to demonstrate the superiority of these methods in terms of accuracy, robustness and speed.

5.4 Classification

Classification, a supervised learning problem, involves predicting the class/label of an unlabeled signal based on a training set comprising of labeled signals. Once features have been extracted and dimensionality reduction applied, the whole feature-set is split into two folds – training set and testing set. While the training set is used to learn decision boundaries defining the class membership of each of the examples, it is through classification of unseen test examples that the performance of the classifier is assessed. Among a number of quantitative measures used to evaluate the performance of the

classifier are accuracy, recall, precision and f-score.

$\text{Accuracy} = \frac{tp + tn}{tp + fp + tn + fn}$	$\text{Precision} = \frac{tp}{tp + fp}$
$\text{Recall} = \frac{tp}{tp + fn}$	$\text{F} = \frac{precision \cdot recall}{precision + recall}$

Table 5.1: A few quantitative measures for performance evaluation of classifiers

Table 5.1 presents equations of each of these evaluation metrics for a simplified case of a 2-class (positive and negative) problem, where *tp* stands for a number of positive examples (truly) predicted as positive, *tn* for a number of negative examples (truly) predicted as negative, *fp* for a number of negative examples (falsely) predicted as positive and *fn* for a number of positive examples (falsely) classified as negative. For visualization and ease of interpretation, these four outcomes can also be presented in a 2×2 contingency table or confusion matrix form (Figure 5.2).

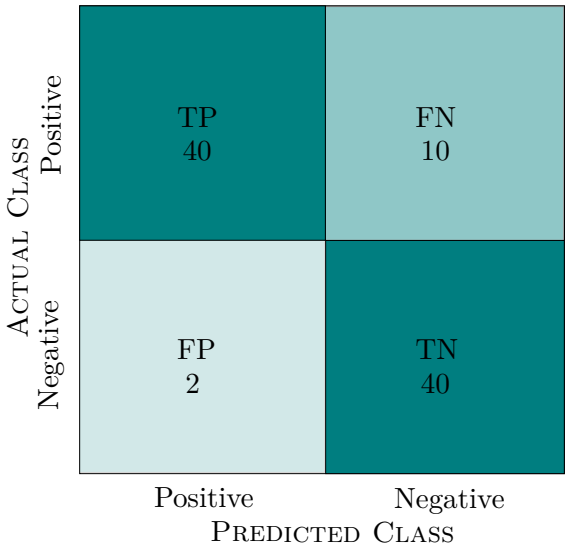

Figure 5.2: An example confusion matrix for a binary classifier. In this particular case, the test set was made up of 92 examples, among them 42 were predicted as 'positive' and 50 were predicted as 'negative'.

Several optimization techniques exist to solve both binary and multi-class classification problems related to NIRS. [108], for instance, presents a study investigating the activation of motor cortex during hand motor imagery that used Fisher's Linear Discriminant Analysis (FLDA) to compare simple and complex finger-tapping tasks. A similar study [67] compared two different classifiers i.e. a Support Vector Machine (SVM) and a Hidden Markov Model (HMM) based on how accurately does each of them classify right

and left-hand motor imagery. Another research [86] involving locked-in patients used non-linear discriminant classifier to differentiate between high-level mental tasks corresponding to 'yes' and 'no'. In the same way, [10] has used both FLDA and SVM to successfully classify visually-cued positively and negatively-valanced emotional induction tasks and [115] has used FLDA to differentiate between neural correlates of preference evaluation related to two different drinks.

Chapter 6

Solution Approach

In chapter 5, a generic pipeline for pre-processing and classification of NIRS signals have been presented and recent trends related to each of the building blocks have been reported. This chapter explains the basis and working principle of the techniques that have been used *in this study* to optimize the classification of overt and covert speech events.

6.1 Data Preparation

When a mental activity is performed, it results in a significant increase in the cerebral blood flow of the relevant area/s of the brain which then appears in the form of an overall localized increase in oxygenated hemoglobin (O2Hb) and a relatively smaller decrease in deoxygenated hemoglobin (HHb). As discussed briefly in § 3.3, in order to convert the attenuation of the received NIR radiation into changes in concentration of O2Hb/HHb, the modified Beer-Lambert law is used. This section presents details of the modified Beer-Lambert relationship and describes a few steps that have been followed so as to prepare the data for preprocessing and feature extraction.

Recall that one trial for a speech event such as overt UP is represented as 12 light intensity recordings (12 channels). Each of these recordings can be converted to changes in optical density as follows:

$$OD = log\frac{I_I}{I_D} \tag{6.1.1}$$

where,

OD: optical density

I_I: incident light intensity

I_D: detected light intensity

According to Beer-Lambert relationship, OD is directly proportional to the extinction coefficient for molar concentration ϵ of the absorber, the concentration c of the absorber and the optical path length L of the light through the absorber.

$$OD = \epsilon cL \tag{6.1.2}$$

In a similar way, changes in optical density i.e. ΔOD can be calculated from a measured change in light attenuation before and after an activation event as follows:

$$\Delta OD = log\frac{I_B}{I_A} \tag{6.1.3}$$

where,

I_B: light intensity measured in baseline condition

I_A: light intensity measured in activation condition

For light traveling through a highly scattering medium, the Beer-Lambert relationship has to be modified to include a term for scattering losses G and a scaling factor so as to make up for increase in optical path length due to scattering. The optical path length L is thus expressed as a product of source-detector distance r and a multiplier ζ, known as the differential path length factor (DPF).

$$OD = log\frac{I_I}{I_D} = \epsilon cr\zeta + G \tag{6.1.4}$$

Assuming scattering losses to be constant over time [116], changes in optical density ΔOD can be expressed based on a measured change in attenuation of light before and after an activation condition as follows:

$$\Delta OD = log\frac{I_B}{I_A} = \epsilon cr\zeta \tag{6.1.5}$$

For a medium containing several different absorbers, total change in light attenuation is expressed as a linear sum of contributions from each of the absorbers. Since the

absorbers of NIR in cerebral tissue are O2Hb and HHb, eq. 6.1.5 can be further expanded as follows:

$$\Delta OD = \{\epsilon_{O2Hb}\Delta[O2Hb] + \epsilon_{HHb}\Delta[HHb]\}r\zeta \tag{6.1.6}$$

If several absorbers at several different wavelengths are to be tested, modified Beer-Lambert law can easily be expanded into a series of equations.

$$\Delta OD^{\lambda_1} = \{\epsilon^{\lambda_1}_{O2Hb}\Delta[O2Hb] + \epsilon^{\lambda_1}_{HHb}\Delta[HHb]\}r\zeta^{\lambda_1} \tag{6.1.7}$$

$$\Delta OD^{\lambda_2} = \{\epsilon^{\lambda_2}_{O2Hb}\Delta[O2Hb] + \epsilon^{\lambda_2}_{HHb}\Delta[HHb]\}r\zeta^{\lambda_2} \tag{6.1.8}$$

Using these simultaneous equations and DPF as calculated by eq. 6.1.9 [117], the chemical concentration of O2Hb and HHb in the biological tissue can be calculated as shown in eq. 6.1.10 and 6.1.11.

$$\zeta = 4.99 + 0.067 \cdot age^{0.814} \tag{6.1.9}$$

$$\Delta[O2Hb] = \frac{\epsilon^{\lambda_2}_{HHb}(\Delta OD^{\lambda_1}/\zeta^{\lambda_1}) - \epsilon^{\lambda_1}_{HHb}(\Delta OD^{\lambda_2}/\zeta^{\lambda_2})}{r(\epsilon^{\lambda_2}_{HHb}\epsilon^{\lambda_1}_{O2Hb} - \epsilon^{\lambda_1}_{HHb}\epsilon^{\lambda_2}_{O2Hb})} \tag{6.1.10}$$

$$\Delta[HHb] = \frac{\epsilon^{\lambda_2}_{O2Hb}(\Delta OD^{\lambda_1}/\zeta^{\lambda_1}) - \epsilon^{\lambda_1}_{O2Hb}(\Delta OD^{\lambda_2}/\zeta^{\lambda_2})}{r(\epsilon^{\lambda_1}_{HHb}\epsilon^{\lambda_2}_{O2Hb} - \epsilon^{\lambda_2}_{HHb}\epsilon^{\lambda_1}_{O2Hb})} \tag{6.1.11}$$

Fig. 6.1 shows a representative example of variation in localized HHb as measured using NIRS from channel # 1 of subject # 1 in response to different overt and covert events.

6.2 Artifact Removal

Each of the NIRS signals was converted into change in concentration of O2Hb and HHb using a set of steps as presented in detail in section 6.1. Artifact removal involves linear detrending of these signals so as to remove a linearly increasing baseline as reported in an earlier study by [97]. A filter was applied to remove linear trends in the metabolic response by minimizing the least-squares error in each session and subsequently subtracting this trend (see Fig. 6.2).

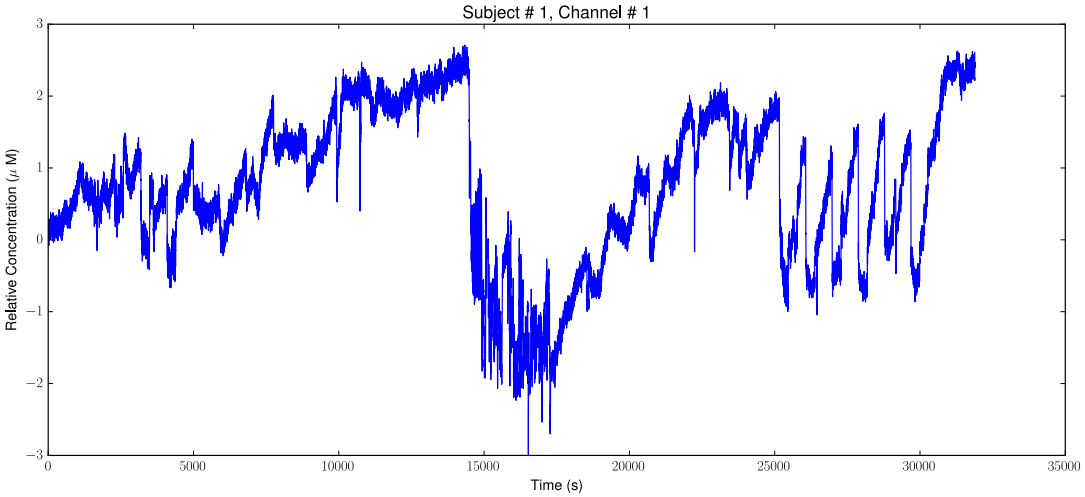

Figure 6.1: Variation in HHb as measured using NIRS from 1^{st} channel of the 1^{st} subject

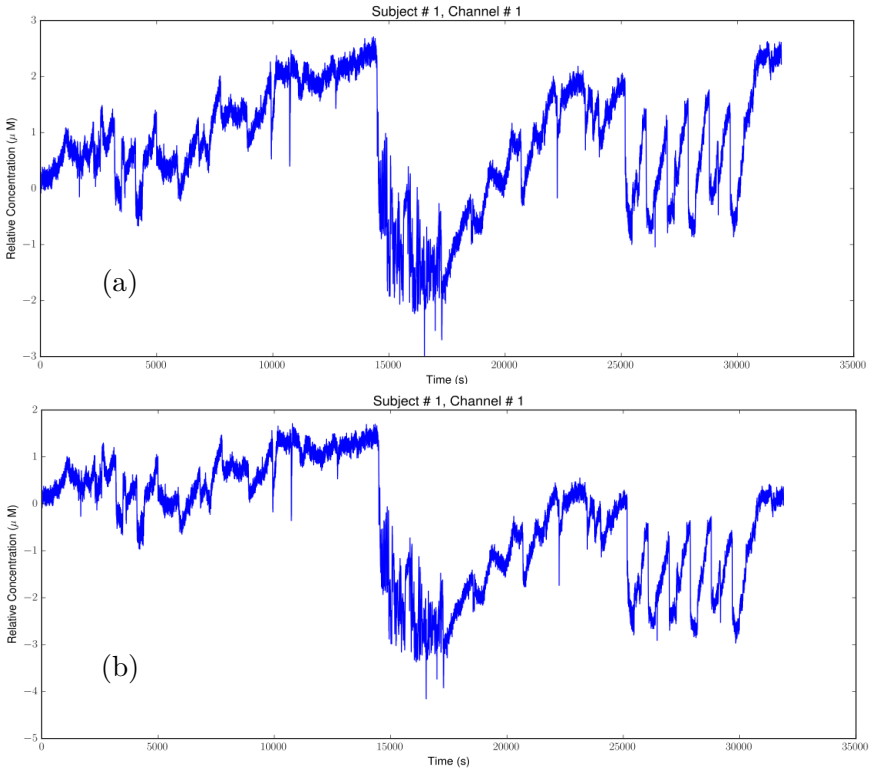

Figure 6.2: HHb response corresponding to the 1^{st} channel of the 1^{st} subject (a) before linear detrending and (b) after linear detrending

6.3 Data Analysis

We are interested in the data analysis of NIRS signals (see Fig. 6.1) of 8 subjects that they have generated in response to different baseline and activation events. Inferential

statistics allow us to use the recorded sample trials to make reasoning about the general trends and tendencies between channels and events. The analysis was performed both within each subject (intra-subject) and across all subjects (across-subjects) based on two of the signal characteristics i.e. peak-to-peak value and correlation.

Across subjects, two combinations of two measures were recorded for each of these signal characteristics. So, for peak-to-peak value, a mean value across all channels (mean_{ch}) was recorded for each of the events and a mean value across all events (mean_{ev}) was recorded for each of the channels. Similarly, a maximum peak-to-peak value across all channels (max_{ch}) was recoded for each of the events and a maximum value across all events (mean_{ev}) was recorded for each of the channels.

6.3.1 Peak-to-peak Value

The peak-to-peak value refers to a difference between the lowest and the highest value within an event (see Fig. 6.3) for each channel and thus contains information about the magnitude of a response during an event. It can be used to determine the channels with relatively high response and thus find out the cerebral location and relevant event that elicits the highest response. The absolute difference between the peak-to-peak value of corresponding events in block one and two (see § 4.2.2) can also be used to test for similarity of events in terms of magnitude of response.

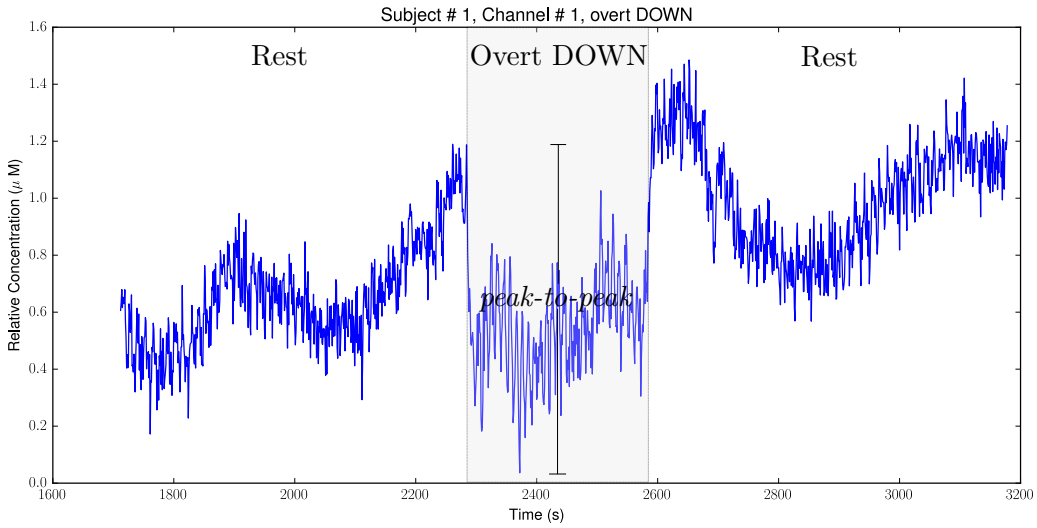

Figure 6.3: Variation in HHb as measured using NIRS for overt DOWN from 1^{st} channel of the 1^{st} subject

The intra-subject global peak-to-peak mean value for one representative subject – subject # 1 – was 2.65 μM (range: 0.65-13.16 μM) for O2Hb and 1.52 μM (range: 0.23-6.88 μM) for HHb. For all subjects, the response for O2Hb turned out to be statistically significantly higher than that for HHb ($p < 0.001$) (see Fig. 6.4).

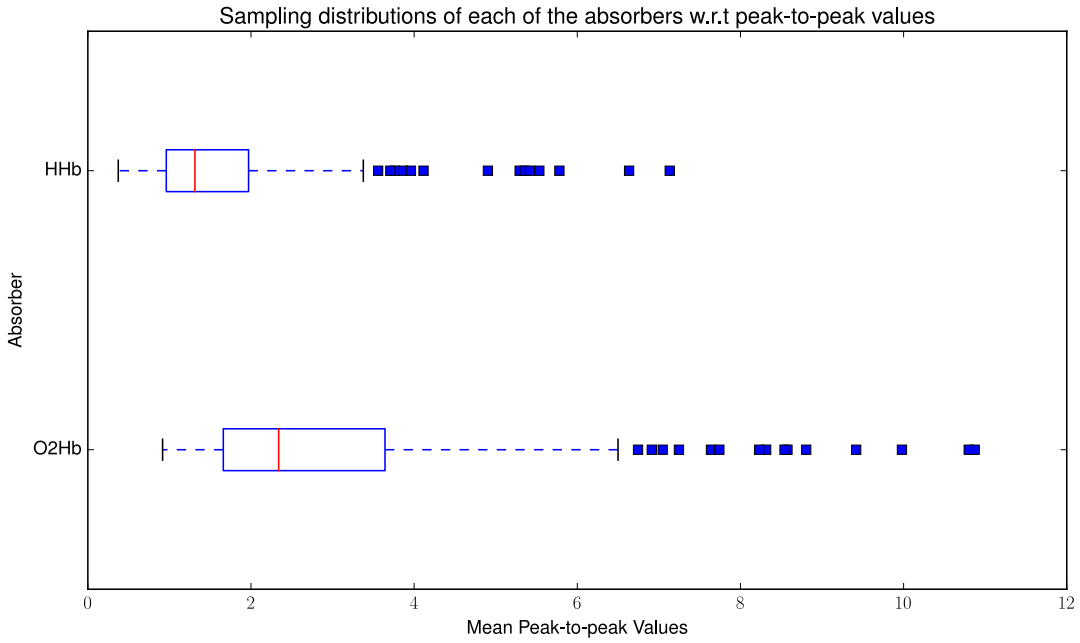

Figure 6.4: Sampling distributions of each of the absorbers – O2Hb and HHb – w.r.t peak-to-peak values

Difference in Channels:

On channel # 7 (covers Broca's area the most), the intra-subject mean (across events) peak-to-peak value for one representative subject – subject # 1 – was 2.74 μM (range: 1.49-5.35 μM) for O2Hb and 1.58 μM (range: 0.53-4.20 μM) for HHb. Discriminating between channels covering Broca's area (4, 6, 7 and 8) and the remaining 8 channels of subject # 1, significant tendencies towards both higher (1 subject, $p < 0.05$) and lower (2 subjects, $p < 0.01$) values were found for both O2Hb and HHb.

Across subjects, mean_{ev} and maximum_{ev} peak-to-peak value for channel # 7 turned out to be 2.54 μM (range: 1.14-5.61 μM) and 7.63 μM (range: 2.92-17.94 μM) respectively. Similar results were obtained for the remaining channels and second block with no significant differences from channel # 7 ($p > 0.05$). The channel providing the maximum value for each event was channel # 8 (see Fig. 6.5), which most frequently represented the highest value (37% of the time), followed by channel # 12 (13% of the time).

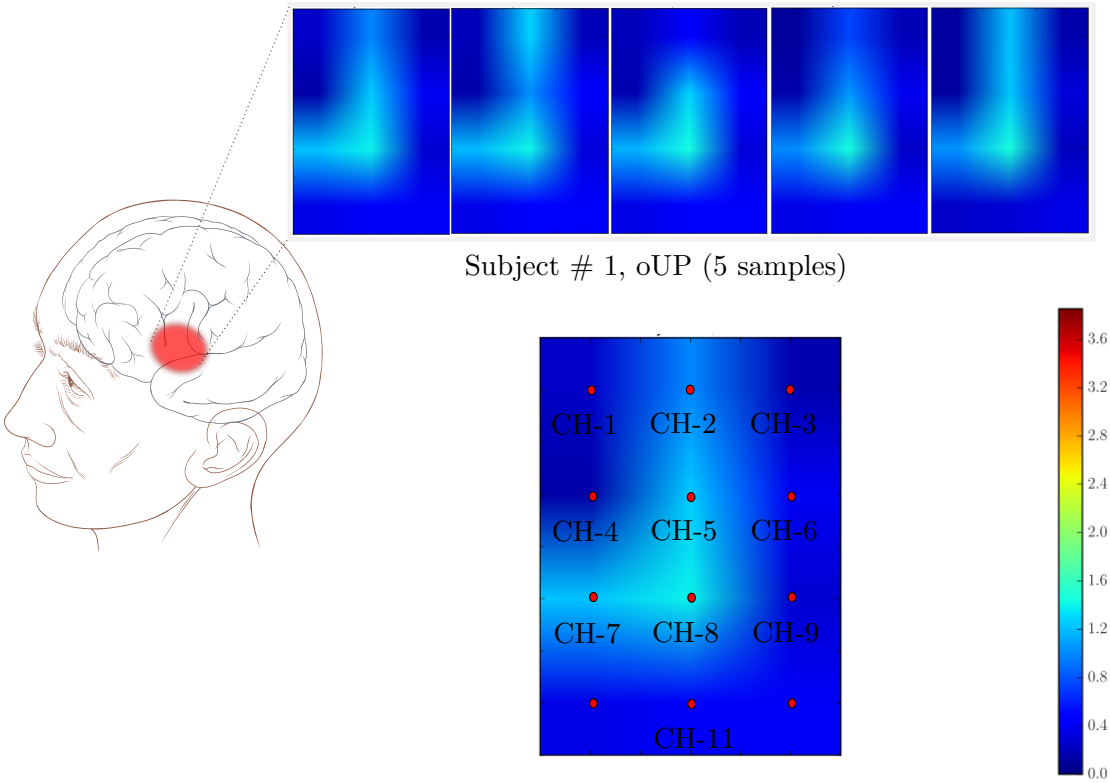

Figure 6.5: This figure presents a few topographical maps for HHb response for 5 samples of overt UP from subject # 1 and a labeled map showing placement of each of the 12 channels. It can be seen that the channel providing maximum value for each of these samples is channel # 8

Difference in Events:

Considering the intra-subject difference between channels during the same event, the mean_{ch} peak-to-peak value for one representative subject – subject # 1 – during the event overt UP was 1.77 μM (range: 0.47-4.03 μM). A statistically significant difference between overt and covert speech was found for both block one and two for all subjects ($p < 0.002$ and $p < 0.004$ respectively) excluding block one for three subjects ($p = 0.93$ for one of them, $p \leq 0.07$ for the remaining two). For five subjects, the mean peak-to-peak value was higher during overt speech as compared to covert speech. In the remaining three subjects, this was only true for one of the two blocks with no unique correlation to their handedness or the order of the overt and covert sessions during the experiment. However, a tendency towards a larger distance between the sample means was observed if overt events precede covert events (0.5 μM) than if it is the other way around (0.3 μM).

Across subjects, mean_{ch} and maximum_{ch} peak-to-peak value for block one for one representative event – overt UP – was 3.46 μM (range: 1.10-6.63 μM) and 8.91 μM (range: 3.18-19.69 μM) respectively. The mean peak-to-peak value was 2.06 μM (range: 0.73-6.19 μM) for overt events and 1.14 μM (range: 0.34-3.78 μM) for covert events with a significant difference between the two groups for block one ($p < 0.003$) and two ($p < 0.001$).

The event providing the maximum value for each channel most frequently was overt RIGHT (20% of time), followed by overt BACKWARD (15%); in general, overt events accounted for 60% of these cases.

6.3.2 Correlation

The correlation between corresponding events of block one and two, determined by the R^2-value, can be used as a measure for similarity of events in terms of shape for a single channel. Combined with the information about the peak-to-peak value, the correlation can be used to test the replicability of the events on the same channels and the suitability of the channels.

The intra-subject global correlation coefficient (R^2) mean value for one representative subject – subject # 1 – was 0.33 μM (range: 0.00-0.89 μM) for O2Hb and 0.29 μM (range: 0.00-0.95 μM) for HHb. Statistically significant differences between O2Hb and HHb were found with both higher (2 subjects, $p < 0.02$) and lower (1 subject, $p = 0.08$) R^2-values.

Difference in Channels:
The mean R^2 for channel # 7 of one representative subject – subject # 1 – was 0.41 μM (range: 0.04-0.79 μM) for O2Hb which was significantly different from two other channels ($p < 0.03$). For HHb, the mean R^2-value for the same channel was 0.60 μM (range: 0.18-0.95 μM) which was significantly different from 8 other channels ($p < 0.04$). Similar results could be obtained for the remaining subjects.

Across subjects, the mean_{ev} and maximum_{ev} R^2-value for one representative channel – channel # 7 – was 0.32 μM (range: 0.18-0.52 μM) and 0.84 μM (range: 0.49-0.93 μM) respectively for O2Hb and 0.33 μM (range: 0.26-0.60 μM) and 0.81 μM (range: 0.60-0.95 μM) respectively for HHb with no significant difference with other channels.

Looking at which channel provided the best correlation for each event, indicating the area with the most similar responses, channel # 4 most frequently represented the highest value (20% of the time for all subjects), followed by channel # 8 (13% of the time) with large intra-subject variation.

Difference in Events:

The intra-subject mean R^2-value for one representative subject – subject # 1 – for one representative event – overt UP – was 0.54 μM (range: 0.15-0.85 μM) for O2Hb and 0.43 μM (range: 0.00-0.88 μM) for HHb with significant difference with four covert events ($p < 0.05$). No such statistically significant difference was found for the remaining subjects.

Across subjects, the mean_{ch} and maximum_{ch} R^2-value for the event overt UP was 0.37 μM (range: 0.10-0.61 μM) and 0.71 μM (range: 0.41-0.92 μM) respectively. Overt events in general had higher R^2-values ($R^2 = 0.33$) than covert events ($R^2 = 0.31$) with no significant difference ($p = 0.74$).

Looking at which event provided the maximum value for each channel, covert UP most frequently represented the highest value (17% of the time for all subjects), followed by overt UP (11% of the time); in general, overt events accounted for 43% of these cases.

6.4 Unsupervised Feature Extraction

Most of the studies to date have focused on a single channel at a time, [108] used a best combination of hand-crafted features such as mean, variance, skewness and kurtosis to differentiate between simple and complex motor imagery finger tapping. For multiple channels, one-dimensional features like root mean square value of all channels can easily be used, [118] created a topographical representation based on two dimensional linear cubic spline interpolation of the rms values of each channel and used ratios such as relative area (eq. 6.4.1) and relative width (eq. 6.4.2) as features.

$$relative\ area = \frac{high\ activity\ area}{total\ topographical\ area} \tag{6.4.1}$$

$$relative\ width = \frac{high\ activity\ width}{total\ topographical\ width} \tag{6.4.2}$$

We don't know what aspects of the NIRS signals are critical to discrimination of overt and covert speech. An information theory based approach may allow an insight into the

information content of the signals. One such unsupervised feature extraction scheme involves finding principal components of a set of speech trials. These principal components are then ordered with each of them accounting for a different level of variation among speech events. These principal components can be thought of as a set of features that describe the variation in all speech events. Features learned this way may or may not be directly related to our hand-crafted features.

Each speech trial can be represented as a combination of principal components and can also be approximated using only the n best principal components. The proposed approach for feature extraction goes as follows:

1. Split the whole dataset into train (first 80% of trials of each of the events) and test sets (last 20% of trials of each of the events)
2. Calculate the principal components from the train set and keep only the first n components that account for the most variation in the set
3. Calculate the feature vectors for each of the training examples by projecting the corresponding trials onto the n-dimensional feature space
4. To extract features of a test speech trial, a set of weights based on the trial and the n-dimensional feature space is calculated by projecting the test trial onto each of the principal components

To preprocess the raw speech signals so as to remove redundancy in data, whitening was applied. An algorithm based on randomized singular value decomposition was used for principal component analysis. This approach, also known as Randomized PCA, is inspired by [113, 114] and uses random sampling to pick out a subspace that accurately approximates the input. In many cases, it turns out to be better than its classical counterparts in terms of accuracy, speed and robustness. It is simple, effective and can be reorganized for maximum performance in a variety of computational architectures.

6.5 Speech Classification

Each NIRS trial corresponds either to a baseline or an activation event. An inherent assumption of the classification problem is that the classes are disjoint; hence, the input

feature space can be divided into many different regions separated by decision boundaries. In order to evaluate the performance of the proposed brain-computer interface, several combinations of classes were investigated for each of the subjects and absorbers. These include:

- Overt and covert events, regardless of the words, resulting in 2 classes (DiffOvCov)
- All overt events separately, resulting in 6 classes (SepOv)
- All covert events separately, resulting in 6 classes (SepCov)

Support Vector Machine (SVM), a supervised learning algorithm, was used for classification in each of these problems. This optimization technique searches for parameter values that maximize the gap between decision boundaries and neighboring points of each of the classes. The larger the margin, the lower the generalization error of the classifier.

Given a training set of feature vectors (x) and corresponding labels (y),

$$(x_i, y_i), i = 1, 2, 3, ..., m \text{ where } x_i \in R^n \text{ and } y \in \{1, 0\}^m \tag{6.5.1}$$

SVM seeks the solution of

$$\min_{w,b,\xi} \frac{1}{2} w^T w + C \sum_{i=1}^{m} \xi_i \tag{6.5.2}$$

such that $y_i(w^T \phi(x_i) + b) \geq 1 - \xi_i$ and $\xi_i \geq 0$.

Here, training feature vectors are mapped to a higher dimensional space using a function ϕ and then a separating hyperplane is found while maximizing the margin. C is the penalty parameter of the error term and $K(x_i, x_j) = \phi(x_i)^T \phi(x_j)^T$ is the kernel function. Among well-known kernels are:

- linear: $K(x_i, x_j) = x_i^T x_j$
- polynomial: $K(x_i, x_j) = (\gamma x_i^T x_j + r)^d, \gamma > 0$
- radial basis function: $K(x_i, x_j) = exp(-\gamma \left\| x_i - x_j \right\|^2), \gamma > 0$

where γ, r and d are kernel parameters.

A one-vs-rest classifier based on SVM was fit on 80% of the trials and tested on the remaining 20%. In training phase, a single classifier per class was trained with feature

vectors related to that particular class labeled as 1 and those related to remaining classes labeled as 0. In testing phase, all classifiers were applied to an unlabeled trial and the label for which the classifier reports the highest confidence score was picked as the best label of the corresponding feature vector. A Gaussian RBF kernel was selected due to a number of reasons including:

- Unlike linear kernel, it can also handle the cases where the relationship between features and labels is non-linear
- It has a fewer hyperparameters than polynomial kernel, and
- It also has a fewer numerical difficulties.

In order to search for the best C and γ, two-dimensional grid-search cross-validation was implemented. Different pairs of C and γ were tried and the one with the best cross-validation accuracy was picked. The performance of the trained SVM model was evaluated based on measures such as accuracy, recall, precision and f1-score (see § 5.4).

Chapter 7

Results

This section presents a few results of the proposed feature extraction and classification pipeline based on evaluation measures as defined in § 5.4, discussion of these results and finally, the conclusion of the study.

7.1 Results

The mean and standard deviation of classification accuracy, recall, precision and f1-score as calculated across all subjects for each of the classification problems – DiffOvCov, SepOv and SepCov (see § 6.5) – are presented in table 7.1 and 7.2.

Task	Accuracy	Recall	Precision	F1-score
DiffOvCov	94.22 ± 6.87	95.26 ± 5.28	93.82 ± 8.59	94.42 ± 6.44
SepOv	58.90 ± 27.68	58.90 ± 27.68	58.77 ± 31.64	56.35 ± 29.61
SepCov	65.91 ± 16.89	65.91 ± 16.89	69.23 ± 17.54	63.51 ± 18.05

Table 7.1: The table shows mean classification accuracy, recall, precision and f1-score across all subjects for each of the combination of classes with O2Hb as an absorber

Confusion matrices for each of the classification problems and absorbers are presented in Fig. 7.1, 7.2 and 7.3.

Task	Accuracy	Recall	Precision	F1-score
DiffOvCov	95.83 ± 5.87	97.54 ± 5.24	94.46 ± 6.57	95.95 ± 5.73
SepOv	66.48 ± 17.07	66.48 ± 17.07	71.74 ± 16.71	64.83 ± 18.11
SepCov	70.08 ± 12.11	70.08 ± 12.11	70.44 ± 12.45	67.22 ± 12.37

Table 7.2: The table shows mean classification accuracy, recall, precision and f1-score across all subjects for each of the combination of classes with HHb as an absorber

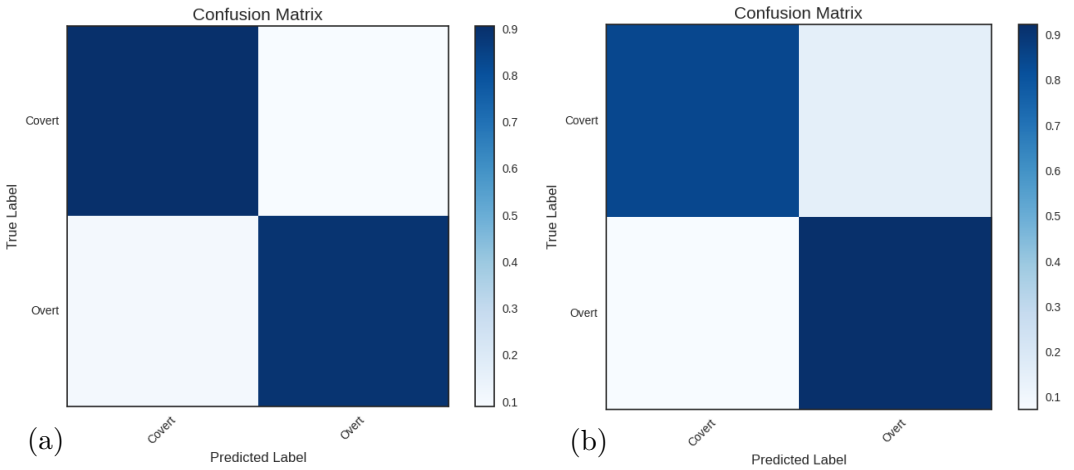

Figure 7.1: Confusion matrix for DiffOvCov with (a) O2Hb (b) HHb as an absorber

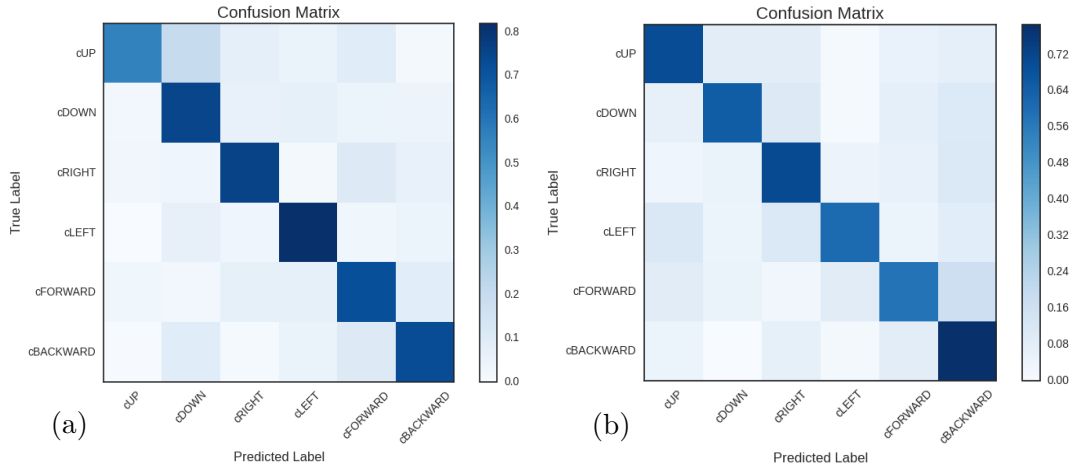

Figure 7.2: Confusion matrix for SepCov with (a) O2Hb (b) HHb as an absorber. cUP here stands for covert UP.

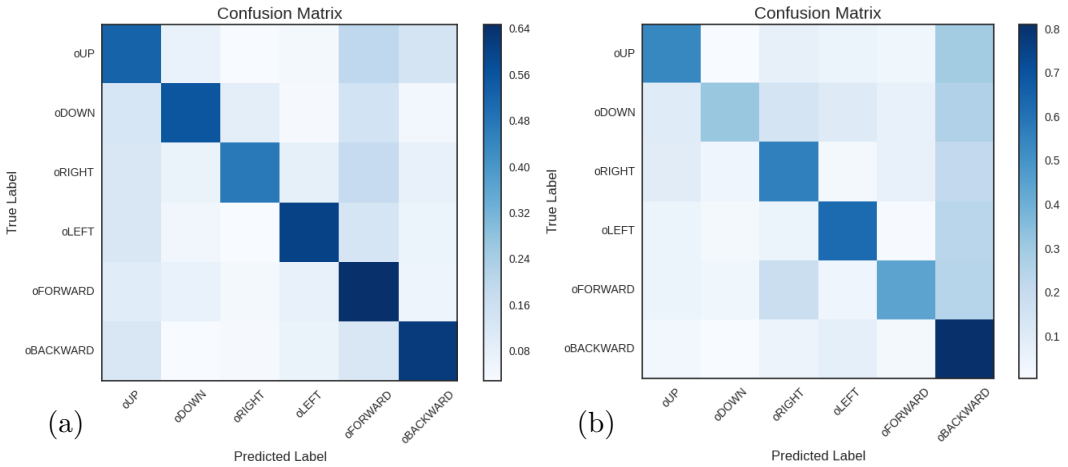

Figure 7.3: Confusion matrix for SepOv with (a) O2Hb (b) HHb as an absorber. oUP here stands for overt UP.

7.2 Discussion

Throughout the investigation of the problem statement, several important issues became clear, these are discussed in the following paragraphs.

The analysis of signals showed that the peak-to-peak values are significantly larger for O2Hb as compared to HHb (see Fig. 6.4), which is similar to findings by other NIRS-based studies [83, 108, 119]. Both absorbers showed similar tendencies throughout the analysis, thus one of them could potentially be chosen for the relevant application. This has also been done by others, where typically O2Hb is mostly used due to larger signal amplitudes thus often higher signal to noise ratio [96, 108]. On the basis of the correlation coefficient between corresponding events of block 1 and 2, which to our best knowledge has not been studied before, both absorbers performed equally well, which also supports choosing one absorber over the other.

Whereas channel # 8 dominantly represented the highest peak-to-peak value across all subjects (37% of the time), the same channel also represented the second-highest correlation coefficient (13% of the time). Interestingly, this channel was located approximately on top of the temple, where the muscular temporalis is accessible, and thus disturbance in NIRS due to motion artifacts is unavoidable [85]. If the muscle artifacts were likely the reason behind highest peak-to-peak value, the high correlation coefficients contradict the existence of such effects because these artifacts would result in large discrepancies between corresponding events and thus, a low correlation.

The comparison of responses during overt and covert events across subjects showed a significant difference towards higher peak-to-peak values for overt events. However, as no significant difference was found for the R^2-values, these results indicate that the signals with high amplitude do not provide more replicable events. On the contrary, for two subjects, covert events had significantly better correlation as compared to the one subject for overt events.

In general, the classification outcomes from using O2Hb were similar to those of HHb, which further emphasizes choosing one absorber. All classification accuracies turned out to be higher than classification by chance. The average classification accuracy for each of the combination of classes was comparable to those achieved by [108] in similar studies. They used an LDA classifier to discriminate between motor imagery (MI) simple and complex finger tapping using a 3-channel template around F3 (see Fig. 4.1) on 12 subjects while we used SVM to classify overt and covert speech events using a 12-channel template around T3 and F7 on 8 subjects. They used hand-crafted features such as mean, variance and skewness while we used unsupervised feature selection to extract most discriminant features. They only used a single best performing channel for feature extraction and classification while we used all 12 channels.

The mean classification accuracy for discrimination between overt events (58.90% for O2Hb, 66.48% for HHb) turned out to be lower than that for covert events (65.91% for O2Hb, 70.08% for HHb). And one reason for that might be: The holder for optodes was too inflexible causing them to lift a small amount from skin during overt tasks which gives rise to motion artifacts as well as light from the light sources being reflected on the skin rather than penetrating. Furthermore, light receivers could potentially receive light from other sources in the room, even though all lights were turned off during the whole experiment. Although motion artifacts were not observed in the measurements, it cannot be completely ruled out that they did occur. Similarly, if the optodes only barely lifted from the skin, a negligible increase and decrease of the transmitted and reflected light respectively would be expected which could be indistinguishable from fluctuations caused by the underlying metabolic response.

The inter-subject variability in classification accuracies as conveyed by especially the corresponding standard deviation figures (see table 7.1 and 7.2) can be explained by a number of factors as mentioned by [83]:

1. Different thickness of the skull, thus different penetration depth of the light
2. Varying size of activation sites
3. Diverse metabolic responses including the possibility of more superficial muscles and/or better capillary network at some sites
4. The use of a constant DPF, corrected for age, might not generalize well to all subjects, although similar methods have been used by [83, 108] and [67]

Although the laterality of Broca's area can vary, especially for left handers, as shown in an MRI study by [99], it could not be observed in this study. Another reason of relatively low classification accuracies in SepOv and SepCov problems might be the length of the experiment. Even though it was kept as short as possible, it was still longer than the time any subject could refrain from using their inner voice and consequently unintentionally produce covert speech. Moreover, sitting in a dark room with no lights lit and their eyes closed might leave the subjects in a daydreaming state which was also reported as a source of problem in a similar study by [119].

7.3 Conclusion

NIRS is a relatively low-cost method for non-invasive measurement of metabolic response comparable to methods such as fMRI. As mentioned by [83], it has several advantages, especially for studies using speech as a control source.

1. Both response for O2Hb and HHb can be measured independently,
2. It's relatively noiseless as compared to MRI
3. It has a relatively good signal to noise ratio
4. It has been shown to be useful for overt speech where fMRI often suffers from motion artifacts
5. It has a superior temporal resolution as compared to MRI though is inferior in spatial resolution
6. It has already been used with compact and portable devices, allowing more freedom and measurements in natural environments

Albeit these advantages, the use of NIRS for a BCI is still at a very early stage providing only a small amount of added freedom to those suffering from neuromuscular disorders inducing paralysis of all four limbs. In conclusion, this thesis:

- Presents a study conducted to investigate if an intuitive BCI based on NIRS can be made
- Demonstrates that speech can potentially be harnessed as an intuitive control source for a NIRS-BCI
- Demonstrates that Broca's area can be used to differentiate between overt and covert speech regardless of words with classification accuracies up to 90%
- Demonstrates that Broca's area can be used to differentiate between covertly spoken words with classification accuracies up to 72%
- Demonstrates that Broca's area can be used to differentiate between overtly spoken words with classification accuracies up to 60%

7.4 Future Prospects

The poor spatial resolution of NIRS and relatively large equipment and sensors as compared to EEG has to be overcome to create a system suitable for everyday use. Moreover, even though NIRS has a good temporal resolution, it is still limited by the slower nature of the metabolic BOLD response (often several seconds) as compared to, for example, electrical activity from neurons (almost instantly). Further studies are needed to test other cognitive areas using different feature extraction and classification pipelines. Studies are also needed to determine if the fast BOLD response occurring milli-seconds after the event can be used to create a faster and more reliable BCI.

References

[1] Cancer Research UK. http://www.cancerresearchuk.org/about-cancer/type/brain-tumour/about/the-brain, 2013 (accessed August 4, 2015).

[2] james.mcd.nz. Diagram of human brain showing speech areas. https://commons.wikimedia.org/wiki/File:Brain_Surface_Gyri.svg, 2007 (accessed August 15, 2015).

[3] Electrode locations of international 10-20 system for eeg recording. https://commons.wikimedia.org/wiki/File:21_electrodes_of_International_10-20_system_for_EEG.svg, 2010 (accessed August 26, 2015).

[4] Patrick J. Lynch. Human head and brain diagram. https://commons.wikimedia.org/wiki/File:Human_head_and_brain_diagram.svg, 2006 (accessed August 26, 2015).

[5] Marie-Aurélie Bruno, Caroline Schnakers, François Damas, Frédéric Pellas, Isabelle Lutte, Jan Bernheim, Steve Majerus, Gustave Moonen, Serge Goldman, and Steven Laureys. Locked-in syndrome in children: Report of five cases and review of the literature. *Pediatric Neurology*, 41(4):237–246, 2009.

[6] Eimear Smith and Mark Delargy. Locked-in syndrome. *BMJ: British Medical Journal*, 330(7488):406, 2005.

[7] Emanuela Casanova, Rosa E Lazzari, Sergio Lotta, and Anna Mazzucchi. Locked-in syndrome: Improvement in the prognosis after an early intensive multidisciplinary rehabilitation. *Archives of Physical Medicine and Rehabilitation*, 84(6): 862–867, 2003.

[8] Stefanie Blain, Alex Mihailidis, and Tom Chau. Assessing the potential of electro-

dermal activity as an alternative access pathway. *Medical Engineering & Physics*, 30(4):498–505, 2008.

[9] Steven Laureys, Frédéric Pellas, Philippe Van Eeckhout, Sofiane Ghorbel, Caroline Schnakers, Fabien Perrin, Jacques Berre, Marie-Elisabeth Faymonville, Karl-Heinz Pantke, Francois Damas, et al. The locked-in syndrome: What is it like to be conscious but paralyzed and voiceless? *Progress in Brain Research*, 150:495–611, 2005.

[10] Kelly Tai. *Near-Infrared Spectroscopy Signal Classification: Towards a Brain-Computer Interface*. PhD thesis, University of Toronto, 2008.

[11] Eric C Leuthardt, Gerwin Schalk, Jonathan R Wolpaw, Jeffrey G Ojemann, and Daniel W Moran. A brain-computer interface using electrocorticographic signals in humans. *Journal of Neural Engineering*, 1(2):63, 2004.

[12] Benjamin Blankertz, Claudia Sannelli, Sebastian Halder, Eva M Hammer, Andrea Kübler, Klaus-Robert Müller, Gabriel Curio, and Thorsten Dickhaus. Neurophysiological predictor of smr-based bci performance. *NeuroImage*, 51(4):1303–1309, 2010.

[13] Jeremy I Skipper, Susan Goldin-Meadow, Howard C Nusbaum, and Steven L Small. Speech-associated gestures, broca's area, and the human mirror system. *Brain and Language*, 101(3):260–277, 2007.

[14] Barry Horwitz, Katrin Amunts, Rajan Bhattacharyya, Debra Patkin, Keith Jeffries, Karl Zilles, and Allen R Braun. Activation of broca's area during the production of spoken and signed language: A combined cytoarchitectonic mapping and pet analysis. *Neuropsychologia*, 41(14):1868–1876, 2003.

[15] Bernhard Obermaier, GR Muller, and Gert Pfurtscheller. "virtual keyboard" controlled by spontaneous eeg activity. *IEEE Transactions on Neural Systems and Rehabilitation Engineering*, 11(4):422–426, 2003.

[16] Tianyou Yu, Yuanqing Li, Jinyi Long, and Zhenghui Gu. Surfing the internet with a bci mouse. *Journal of Neural Engineering*, 9(3):036012, 2012.

[17] Brice Rebsamen, Chee Leong Teo, Qiang Zeng, Marcelo H Ang Jr, Etienne Burdet, Cuntai Guan, Haihong Zhang, and Christian Laugier. Controlling a wheelchair indoors using thought. *Intelligent Systems, IEEE*, 22(2):18–24, 2007.

[18] S Saladin Kenneth and MP Carol. *Anatomy and Physiology: The Unity of Form and Function*. McGraw-Hill. Boston, Massachusetts, USA, 1998.

[19] Kalyani Premkumar. *The Massage Connection: Anatomy and Physiology*. Lippincott Williams & Wilkins, 2004.

[20] Robert K Clark. *Anatomy and Physiology: Understanding the Human Body*. Jones & Bartlett Learning, 2005.

[21] W. Arnould-Taylor. *A Textbook of Anatomy and Physiology*. Stanley Thornes, 1998. ISBN 9780748736348.

[22] J. Seikel, D. King, and D. Drumright. *Anatomy & Physiology for Speech, Language, and Hearing*. Cengage Learning, 2015. ISBN 9781305687998.

[23] Frederic H. Martini. *Fundamentals of Anatomy & Physiology*. Pearson, 2005. ISBN 9780805372809.

[24] S. Standring. *Gray's Anatomy - The Anatomical Basis of Clinical Practice*. Churchill Livingstone, 1999.

[25] D. Coon. *Psychology: A Modular Approach to Mind and Behavior*. Advantage Series. Cengage Learning, 2005. ISBN 9780534605933.

[26] Julius Fridriksson, H Isabel Hubbard, Sarah Grace Hudspeth, Audrey L Holland, Leonardo Bonilha, Davida Fromm, and Chris Rorden. Speech entrainment enables patients with broca's aphasia to produce fluent speech. *Brain*, 135(12):3815–3829, 2012.

[27] NF Dronkers, JK Shapiro, B Redfern, and RT Knight. The role of broca's area in broca's aphasia. *Journal of Clinical and Experimental Neuropsychology*, 14(52-53), 1992.

[28] JP Mohr, MS Pessin, S Finkelstein, HH Funkenstein, GW Duncan, and KR Davis. Broca aphasia pathologic and clinical. *Neurology*, 28(4):311–311, 1978.

[29] NF Dronkers and CA Ludy. Brain lesion analysis in clinical research. *Handbook of Neurolinguistics*, pages 173–187, 1998.

[30] Marcel Adam Just, Patricia A Carpenter, Timothy A Keller, William F Eddy, and Keith R Thulborn. Brain activation modulated by sentence comprehension. *Science*, 274(5284):114–116, 1996.

[31] David Caplan, Nathaniel Alpert, Gloria Waters, and Anthony Olivieri. Activation of broca's area by syntactic processing under conditions of concurrent articulation. *Human Brain Mapping*, 9(2):65–71, 2000.

[32] Marco Iacoboni, Roger P Woods, Marcel Brass, Harold Bekkering, John C Mazziotta, and Giacomo Rizzolatti. Cortical mechanisms of human imitation. *Science*, 286(5449):2526–2528, 1999.

[33] Ferdinand Binkofski, Katrin Amunts, Klaus Martin Stephan, Stefan Posse, Thorsten Schormann, Hans-Joachim Freund, Karl Zilles, and Rüdiger J Seitz. Broca's region subserves imagery of motion: A combined cytoarchitectonic and fmri study. *Human Brain Mapping*, 11(4):273–285, 2000.

[34] Nikos K Logothetis, Jon Pauls, Mark Augath, Torsten Trinath, and Axel Oeltermann. Neurophysiological investigation of the basis of the fmri signal. *Nature*, 412 (6843):150–157, 2001.

[35] Arien J Smith, Hal Blumenfeld, Kevin L Behar, Douglas L Rothman, Robert G Shulman, and Fahmeed Hyder. Cerebral energetics and spiking frequency: The neurophysiological basis of fmri. *Proceedings of the National Academy of Sciences*, 99(16):10765–10770, 2002.

[36] Scott A Huettel, Allen W Song, and Gregory McCarthy. *Functional Magnetic Resonance Imaging*, volume 1. Sinauer Associates Sunderland, 2004.

[37] Richard B Buxton. *Introduction to Functional Magnetic Resonance Imaging: Principles and Techniques*. Cambridge University Press, 2009.

[38] Amir Shmuel, Mark Augath, Axel Oeltermann, and Nikos K Logothetis. Negative functional mri response correlates with decreases in neuronal activity in monkey visual area v1. *Nature Neuroscience*, 9(4):569–577, 2006.

[39] Nikolaus Weiskopf, Ranganatha Sitaram, Oliver Josephs, Ralf Veit, Frank Scharnowski, Rainer Goebel, Niels Birbaumer, Ralf Deichmann, and Klaus Mathiak. Real-time functional magnetic resonance imaging: Methods and applications. *Magnetic Resonance Imaging*, 25(6):989–1003, 2007.

[40] G Rota, R Sitaram, R Veit, N Weiskopf, N Birbaumer, and G Dogil. fmri-neurofeedback for operant conditioning and neural plasticity investigation: A study on the physiological self-induced regulation of the ba 45. In *Proceedings of the Cognitive Neuroscience Conference*, 2006.

[41] Frank Tong, Ken Nakayama, J Thomas Vaughan, and Nancy Kanwisher. Binocular rivalry and visual awareness in human extrastriate cortex. *Neuron*, 21(4): 753–759, 1998.

[42] Seung-Schik Yoo, Ty Fairneny, Nan-Kuei Chen, Seh-Eun Choo, Lawrence P Panych, HyunWook Park, Soo-Young Lee, and Ferenc A Jolesz. Brain-computer interface using fmri: Spatial navigation by thoughts. *NeuroReport*, 15(10):1591–1595, 2004.

[43] R Christopher deCharms, Fumiko Maeda, Gary H Glover, David Ludlow, John M Pauly, Deepak Soneji, John DE Gabrieli, and Sean C Mackey. Control over brain activation and pain learned by using real-time functional mri. *Proceedings of the National Academy of Sciences of the United States of America*, 102(51):18626–18631, 2005.

[44] Niels Birbaumer. Breaking the silence: Brain-computer interfaces (bci) for communication and motor control. *Psychophysiology*, 43(6):517–532, 2006.

[45] Ernst Niedermeyer and FH Lopes da Silva. *Electroencephalography: Basic Principles, Clinical Applications, and Related Fields*. Lippincott Williams & Wilkins, 2005.

[46] Paul L Nunez and Ramesh Srinivasan. *Electric Fields of the Brain: The Neurophysics of EEG*. Oxford university press, 2006.

[47] Carmine Pariante. *Understanding Depression: A Translational Approach*. Oxford University Press, 2009.

[48] Ramesh Srinivasan, William R Winter, and Paul L Nunez. Source analysis of eeg oscillations using high-resolution eeg and meg. *Progress in Brain Research*, 159: 29–42, 2006.

[49] Sergio Machado, Fernanda Araújo, Flávia Paes, Bruna Velasques, Mario Cunha, Henning Budde, Luis F Basile, Renato Anghinah, Oscar Arias-Carrión, Mauricio Cagy, et al. Eeg-based brain-computer interfaces: An overview of basic concepts and clinical applications in neurorehabilitation. *Reviews in the Neurosciences*, 21 (6):451–468, 2010.

[50] Andrea Kübler, Femke Nijboer, Jürgen Mellinger, Theresa M Vaughan, Hannelore Pawelzik, Gerwin Schalk, Dennis J McFarland, Niels Birbaumer, and Jonathan R Wolpaw. Patients with als can use sensorimotor rhythms to operate a brain-computer interface. *Neurology*, 64(10):1775–1777, 2005.

[51] Gert Pfurtscheller, C Guger, G Müller, G Krausz, and C Neuper. Brain oscillations control hand orthosis in a tetraplegic. *Neuroscience Letters*, 292(3):211–214, 2000.

[52] Niels Birbaumer, Nimr Ghanayim, Thilo Hinterberger, Iver Iversen, Boris Kotchoubey, Andrea Kübler, Juri Perelmouter, Edward Taub, and Herta Flor. A spelling device for the paralysed. *Nature*, 398(6725):297–298, 1999.

[53] Birbaumer Niels et al. The thought translation device (ttd) for completely paralyzed patients. *IEEE Transactions on Rehabilitation Engineering*, 8(2), 2000.

[54] Dean J Krusienski, Eric W Sellers, François Cabestaing, Sabri Bayoudh, Dennis J McFarland, Theresa M Vaughan, and Jonathan R Wolpaw. A comparison of classification techniques for the p300 speller. *Journal of Neural Engineering*, 3(4): 299, 2006.

[55] Eric W Sellers, Dean J Krusienski, Dennis J McFarland, Theresa M Vaughan, and Jonathan R Wolpaw. A p300 event-related potential brain-computer interface (bci): The effects of matrix size and inter stimulus interval on performance. *Biological Psychology*, 73(3):242–252, 2006.

[56] Jonathan R Wolpaw and Dennis J McFarland. Control of a two-dimensional movement signal by a non-invasive brain-computer interface in humans. *Proceedings*

of the National Academy of Sciences of the United States of America, 101(51): 17849–17854, 2004.

[57] Leonard J Trejo, Roman Rosipal, and Bryan Matthews. Brain-computer interfaces for 1-d and 2-d cursor control: Designs using volitional control of the eeg spectrum or steady-state visual evoked potentials. *Neural Systems and Rehabilitation Engineering, IEEE Transactions on*, 14(2):225–229, 2006.

[58] NV O'Donohoe. The eeg and neuroimaging in the management of the epilepsies. *Archives of disease in childhood*, 73(6):552, 1995.

[59] CM Verity. The place of the eeg and imaging in the management of seizures. *Archives of disease in childhood*, 73(6):557, 1995.

[60] Eric Arthur Pohlmeyer. *A Brain-machine Interface for Regaining Control of a Paralyzed Arm: A Primate Model of Cortically Controlled Functional Electrical Stimulation*. ProQuest, 2008.

[61] Jaime Pineda, David S Silverman, Andrey Vankov, John Hestenes, et al. Learning to control brain rhythms: Making a brain-computer interface possible. *Neural Systems and Rehabilitation Engineering, IEEE Transactions on*, 11(2):181–184, 2003.

[62] Fay S Tyner and John Russell Knott. *Fundamentals of EEG Technology: Basic Concepts and Methods*, volume 1. Lippincott Williams & Wilkins, 1983.

[63] Alexander J Casson. Artificial neural network classification of operator workload with an assessment of time variation and noise-enhancement to increase performance. *Frontiers in Neuroscience*, 8, 2014.

[64] Eiju Watanabe, Yuichi Yamashita, Atsushi Maki, Yoshitoshi Ito, and Hideaki Koizumi. Non-invasive functional mapping with multi-channel near infra-red spectroscopic topography in humans. *Neuroscience Letters*, 205(1):41–44, 1996.

[65] Eiju Watanabe, Atsushi Maki, Fumio Kawaguchi, Kaoru Takashiro, Yuichi Yamashita, Hideaki Koizumi, and Yoshiaki Mayanagi. Non-invasive assessment of language dominance with near-infrared spectroscopic mapping. *Neuroscience Letters*, 256(1):49–52, 1998.

[66] Linda Ko. *Near-infrared Spectroscopy as an Access Channel: Prefrontal Cortex Inhibition during an Auditory Go-No-Go Task*. PhD thesis, 2009.

[67] Ranganatha Sitaram, Haihong Zhang, Cuntai Guan, Manoj Thulasidas, Yoko Hoshi, Akihiro Ishikawa, Koji Shimizu, and Niels Birbaumer. Temporal classification of multichannel near-infrared spectroscopy signals of motor imagery for developing a brain-computer interface. *NeuroImage*, 34(4):1416–1427, 2007.

[68] Gary Strangman, David A Boas, and Jeffrey P Sutton. Non-invasive neuroimaging using near-infrared light. *Biological Psychiatry*, 52(7):679–693, 2002.

[69] Alper Bozkurt, Arye Rosen, Harel Rosen, and Banu Onaral. A portable near infrared spectroscopy system for bedside monitoring of newborn brain. *Biomedical Engineering Online*, 4(1):29, 2005.

[70] JM Murkin and M Arango. Near-infrared spectroscopy as an index of brain and tissue oxygenation. *British Journal of Anaesthesia*, 103(suppl 1):i3–i13, 2009.

[71] Arno Villringer and Britton Chance. Non-invasive optical spectroscopy and imaging of human brain function. *Trends in Neurosciences*, 20(10):435–442, 1997.

[72] Gabriele Gratton, Marsha Ruth Goodman-Wood, and Monica Fabiani. Comparison of neuronal and hemodynamic measures of the brain response to visual stimulation: An optical imaging study. *Human Brain Mapping*, 13(1):13–25, 2001.

[73] John EW Mayhew, Stephen Askew, Ying Zheng, John Porrill, GW Max Westby, Peter Redgrave, David M Rector, and Ronald M Harper. Cerebral vasomotion: A 0.1-hz oscillation in reflected light imaging of neural activity. *NeuroImage*, 4(3): 183–193, 1996.

[74] Gabriele Gratton and Paul M Corballis. Removing the heart from the brain: Compensation for the pulse artifact in the photon migration signal. *Psychophysiology*, 32(3):292–299, 1995.

[75] David T Delpy, Mark Cope, Pieter van der Zee, SR Arridge, Susan Wray, and JS Wyatt. Estimation of optical pathlength through tissue from direct time of flight measurement. *Physics in Medicine and Biology*, 33(12):1433, 1988.

[76] Christina Hirth, Hellmuth Obrig, Kersten Villringer, Andeas Thiel, Johannes Bernarding, Werner Mühlnickel, Herta Flor, Ulrich Dirnagl, and Arno Villringer. Non-invasive functional mapping of the human motor cortex using near-infrared spectroscopy. *NeuroReport*, 7(12):1977–1981, 1996.

[77] Hauke R Heekeren, Matthais Kohl, Hellmuth Obrig, Rüdiger Wenzel, Wolfram von Pannwitz, Steven J Matcher, Ulrich Dirnagl, Chris E Cooper, and Arno Villringer. Non-invasive assessment of changes in cytochrome-c oxidase oxidation in human subjects during visual stimulation. *Journal of Cerebral Blood Flow & Metabolism*, 19(6):592–603, 1999.

[78] Christoph Hock, Kersten Villringer, Franz Müller-Spahn, Rüdiger Wenzel, Hauke Heekeren, Sigrid Schuh-Hofer, Marc Hofmann, Satoshi Minoshima, Markus Schwaiger, Ulrich Dirnagl, et al. Decrease in parietal cerebral hemoglobin oxygenation during performance of a verbal fluency task in patients with alzheimer's disease monitored by means of near-infrared spectroscopy (nirs)âĂŤcorrelation with simultaneous rcbf-pet measurements. *Brain Research*, 755(2):293–303, 1997.

[79] Yoko Hoshi and Mamoru Tamura. Near-infrared optical detection of sequential brain activation in the prefrontal cortex during mental tasks. *NeuroImage*, 5(4): 292–297, 1997.

[80] AJ Fallgatter, Th J Müller, and WK Strik. Prefrontal hypooxygenation during language processing assessed with near-infrared spectroscopy. *Neuropsychobiology*, 37(4):215–218, 1998.

[81] Kaoru Sakatani, Yuxiao Xie, Wemara Lichty, Sunwei Li, and Huancong Zuo. Language-activated cerebral blood oxygenation and hemodynamic changes of the left prefrontal cortex in poststroke aphasic patients: A near-infrared spectroscopy study. *Stroke*, 29(7):1299–1304, 1998.

[82] Hiroki Sato, Tatsuya Takeuchi, and Kuniyoshi L Sakai. Temporal cortex activation during speech recognition: an optical topography study. *Cognition*, 73(3):B55–B66, 1999.

[83] Valentina Quaresima, Marco Ferrari, Marco CP van der Sluijs, Jan Menssen, and Willy NJM Colier. Lateral frontal cortex oxygenation changes during translation

and language switching revealed by non-invasive near-infrared multi-point measurements. *Brain research bulletin*, 59(3):235–243, 2002.

[84] Yasuyo Minagawa-Kawai, Koichi Mori, Izumi Furuya, Ryoko Hayashi, and Yutaka Sato. Assessing cerebral representations of short and long vowel categories by nirs. *NeuroReport*, 13(5):581–584, 2002.

[85] Andrew F Cannestra, Isabell Wartenburger, Hellmuth Obrig, Arno Villringer, and Arthur W Toga. Functional assessment of broca's area using near-infrared spectroscopy in humans. *NeuroReport*, 14(15):1961–1965, 2003.

[86] Masayoshi Naito, Yohko Michioka, Kuniaki Ozawa, Masashi KIGUCHI, and Tsuneo KANAZAWA. A communication means for totally locked-in als patients based on changes in cerebral blood volume measured with near-infrared light. *IEICE transactions on information and systems*, 90(7):1028–1037, 2007.

[87] A Ramos Murguialday, J Hill, M Bensch, S Martens, S Halder, F Nijboer, Bernhard Schoelkopf, N Birbaumer, and A Gharabaghi. Transition from the locked-in to the completely locked-in state: A physiological analysis. *Clinical Neurophysiology*, 122(5):925–933, 2011.

[88] Guillermo Gallegos-Ayala, Adrian Furdea, Kouji Takano, Carolin A Ruf, Herta Flor, and Niels Birbaumer. Brain communication in a completely locked-in patient using bedside near-infrared spectroscopy. *Neurology*, 82(21):1930–1932, 2014.

[89] Nobuo Masataka, Leonid Perlovsky, and Kazuo Hiraki. Near-infrared spectroscopy (nirs) in functional research of prefrontal cortex. *Frontiers in Human Neuroscience*, 9, 2015.

[90] Saeid Sanei and Jonathon A Chambers. *EEG Signal Processing*. John Wiley & Sons, 2013.

[91] Nicola Neumann and Andrea Kübler. Training locked-in patients: A challenge for the use of brain-computer interfaces. *Neural Systems and Rehabilitation Engineering, IEEE Transactions on*, 11(2):169–172, 2003.

[92] Carlo Giussani, F-E Roux, Vincent Lubrano, Sergio M Gaini, and Lorenzo Bello. Review of language organisation in bilingual patients: What can we learn from direct brain mapping? *Acta Neurochirurgica*, 149(11):1109–1116, 2007.

[93] Richard C Oldfield. The assessment and analysis of handedness: The edinburgh inventory. *Neuropsychologia*, 9(1):97–113, 1971.

[94] F Zerrin Yetkin, Thomas A Hammeke, Sara J Swanson, George L Morris, Wade M Mueller, Timothy L McAuliffe, and Victor M Haughton. A comparison of functional mr activation patterns during silent and audible language tasks. *American Journal of Neuroradiology*, 16(5):1087–1092, 1995.

[95] Elizabeth A Phelps, Fahmeed Hyder, Andrew M Blamire, and Robert G Shulman. Fmri of the prefrontal cortex during overt verbal fluency. *NeuroReport*, 8(2):561–565, 1997.

[96] Rachel Hull, Heather Bortfeld, and Susan Koons. Near-infrared spectroscopy and cortical responses to speech production. *The Open Neuroimaging Journal*, 3:26, 2009.

[97] Shirley Coyle. *Near-infrared Spectroscopy for Brain Computer Interfacing*. PhD thesis, National University of Ireland Maynooth, 2005.

[98] Richard W Homan, John Herman, and Phillip Purdy. Cerebral location of international 10–20 system electrode placement. *Electroencephalography and Clinical Neurophysiology*, 66(4):376–382, 1987.

[99] Simon Sean Keller, John Robin Highley, Marta Garcia-Finana, Vanessa Sluming, Roozbeh Rezaie, and Neil Roberts. Sulcal variability, stereological measurement and asymmetry of broca's area on mr images. *Journal of Anatomy*, 211(4):534–555, 2007.

[100] M Schecklmann, AC Ehlis, MM Plichta, and AJ Fallgatter. Influence of muscle activity on brain oxygenation during verbal fluency assessed with functional near-infrared spectroscopy. *Neuroscience*, 171(2):434–442, 2010.

[101] Shirley M Coyle, Tomás E Ward, and Charles M Markham. Brain–computer interface using a simplified functional near-infrared spectroscopy system. *Journal of Neural Engineering*, 4(3):219, 2007.

[102] Robert J Cooper, Juliette Selb, Louis Gagnon, Dorte Phillip, Henrik W Schytz, Helle K Iversen, Messoud Ashina, and David A Boas. A systematic comparison

of motion artifact correction techniques for functional near-infrared spectroscopy. *Frontiers in Neuroscience*, 6, 2012.

[103] Afrouz A Anderson, Elizabeth Smith, Victor Chernomordik, Yasaman Ardeshirpour, Fatima Chowdhry, Audrey Thurm, David Black, Dennis Matthews, Owen Rennert, and Amir H Gandjbakhche. Prefrontal cortex hemodynamics and age: A pilot study using functional near infrared spectroscopy in children. *Frontiers in Neuroscience*, 8, 2014.

[104] Quan Zhang, Emery N Brown, and Gary E Strangman. Adaptive filtering for global interference cancellation and real-time recovery of evoked brain activity: A monte carlo simulation study. *Journal of Biomedical Optics*, 12(4):044014–044014, 2007.

[105] Il-Young Son and Birsen Yazici. Near infrared imaging and spectroscopy for brain activity monitoring. In *Advances in Sensing with Security Applications*, pages 341–372. Springer, 2006.

[106] Kwang Eun Jang, Sungho Tak, Jinwook Jung, Jaeduck Jang, Yong Jeong, and Jong Chul Ye. Wavelet minimum description length detrending for near-infrared spectroscopy. *Journal of Biomedical Optics*, 14(3):034004–034004, 2009.

[107] Loukianos Spyrou, Yvonne Blokland, Jason Farquhar, and Jorgen Bruhn. Singular spectrum analysis as a preprocessing filtering step for fnirs brain computer interfaces. In *Signal Processing Conference (EUSIPCO), 2014 Proceedings of the 22nd European*, pages 46–50. IEEE, 2014.

[108] Lisa Holper and Martin Wolf. Single-trial classification of motor imagery differing in task complexity: A functional near-infrared spectroscopy study. *J Neuroeng Rehabil*, 8(1):34, 2011.

[109] Zhen Yuan. Spatiotemporal and time-frequency analysis of functional near infrared spectroscopy brain signals using independent component analysis. *Journal of Biomedical Optics*, 18(10):106011–106011, 2013.

[110] Paul Addison. A review of wavelet transform time-frequency methods for nirs-based analysis of cerebral autoregulation. 2015.

[111] Christopher M Bishop. *Pattern Recognition and Machine Learning*. springer, 2006.

[112] Franco Woolfe, Edo Liberty, Vladimir Rokhlin, and Mark Tygert. A fast randomized algorithm for the approximation of matrices. *Applied and Computational Harmonic Analysis*, 25(3):335–366, 2008.

[113] Per-Gunnar Martinsson, Vladimir Rokhlin, and Mark Tygert. A randomized algorithm for the decomposition of matrices. *Applied and Computational Harmonic Analysis*, 30(1):47–68, 2011.

[114] Nathan Halko, Per-Gunnar Martinsson, and Joel A Tropp. Finding structure with randomness: Probabilistic algorithms for constructing approximate matrix decompositions. *SIAM Review*, 53(2):217–288, 2011.

[115] Sheena Luu and Tom Chau. Decoding subjective preference from single-trial near-infrared spectroscopy signals. *Journal of Neural Engineering*, 6(1):016003, 2009.

[116] Peter Rolfe. In vivo near-infrared spectroscopy. *Annual review of biomedical engineering*, 2(1):715–754, 2000.

[117] K L M Koenraadt, J Duysens, M Smeenk, and N L W Keijsers. Multi-channel nirs of the primary motor cortex to discriminate hand from foot activity. *Journal of Neural Engineering*, 9(4):046010, 2012.

[118] Stanley HF Siu, Y Hu, and Keith DK Luk. Realization of lumbar muscle activities using quantitative surface electromyographic topography. In *Neural Engineering, 2009. NER'09. 4th International IEEE/EMBS Conference on*, pages 26–29. IEEE, 2009.

[119] Martin J Herrmann, Michael M Plichta, Ann-Christine Ehlis, and Andreas J Fallgatter. Optical topography during a go–nogo task assessed with multi-channel near-infrared spectroscopy. *Behavioural brain research*, 160(1):135–140, 2005.